

Accurate encoding and decoding by single cells: amplitude versus frequency modulation

Gabriele Micali^{1,2,3}, Gerardo Aquino^{1,2}, David M. Richards^{1,2}, and Robert G. Endres^{1,2,*}

¹ Department of Life Sciences, Imperial College, London, UK

² Centre for Integrative Systems Biology and Bioinformatics, Imperial College, London, UK

³ Dipartimento di Fisica, Università degli Studi di Milano, Milano, Italy

* E-mail: r.endres@imperial.ac.uk

Abstract

Cells sense external concentrations and, via biochemical signaling, respond by regulating the expression of target proteins. Both in signaling networks and gene regulation there are two main mechanisms by which the concentration can be encoded internally: amplitude modulation (AM), where the absolute concentration of an internal signaling molecule encodes the stimulus, and frequency modulation (FM), where the period between successive bursts represents the stimulus. Although both mechanisms have been observed in biological systems, the question of when it is beneficial for cells to use either AM or FM is largely unanswered. Here, we first consider a simple model for a single receptor (or ion channel), which can either signal continuously whenever a ligand is bound, or produce a burst in signaling molecule upon receptor binding. We find that bursty signaling is more accurate than continuous signaling only for sufficiently fast dynamics. This suggests that modulation based on bursts may be more common in signaling networks than in gene regulation. We then extend our model to multiple receptors, where continuous and bursty signaling are equivalent to AM and FM respectively, finding that AM is always more accurate. This implies that the reason some cells use FM is related to factors other than accuracy, such as the ability to coordinate expression of multiple genes or to implement threshold crossing mechanisms.

Author Summary

Signals, and hence information, can generally be transmitted either by amplitude (AM) or frequency (FM) modulation, as used, for example, in the transmission of radio waves since the 1930s. Both types of modulation are known to play a role in biology with AM conventionally associated with signaling and gene expression, and FM used to reliably transmit electrical signals over large distances between neurons. Surprisingly, FM was recently also observed in gene regulation, making their roles less distinct than previously thought. Although the engineering advantages and disadvantages of AM and FM are well understood, the equivalent question in biological systems is still largely unsolved. Here, we propose a simple model of signaling by receptors (or ion channels) with subsequent gene regulation, thus implementing both AM and FM in different types of biological pathways. We then compare the accuracy in the production of target proteins. We find that FM can be more accurate than AM only for a single receptor with fast signaling, whereas AM is more accurate in slow gene regulation and with signaling by multiple receptors. Finally, we propose possible reasons that cells use FM despite the potential decrease in accuracy.

Introduction

Cells are exposed to changing environmental conditions and need to respond to external stimuli with high accuracy, e.g. to utilize nutrients and to avoid lethal stresses [1, 2]. To represent (encode) chemicals in the environment, either ligand-bound receptors trigger chemical signals or ion channels allow entry of secondary messengers. These in turn activate transcription factors (TFs), which then regulate target-protein production (decoding). In eukaryotic cells, the conventional view is that the level of signaling within the cell directly encodes the external stimuli, with consequent gradual changes in the nuclear TF concentrations. This is effectively an amplitude modulation (AM) mechanism [3–10]. However, recent single-cell experiments also show pulsating signals [3, 11–14] and bursty entry of TFs into the

nucleus [3, 10, 15–17], in close analogy to frequency modulation (FM). (Note that, although there is no modulation of an underlying carrier wave as in radio broadcasting [18], the AM/FM terminology is commonly used in quantitative biology [10, 15].) Although several hypotheses have been put forward, the benefits and detrimental effects of either type of response remain largely unclear.

There is experimental evidence that both types of modulation occur in gene regulation. For example, take the budding yeast *Saccharomyces cerevisiae*. Under oxidative stress the nuclear concentration of transcription factor Msn2 is proportional to the H_2O_2 concentration, suggesting an AM mechanism (Fig. 1A,B) [10]. However, in response to a calcium stimulus, Crz1, which is normally cytoplasmic, enters the nucleus in unsynchronized bursts, regulating at least a hundred target genes (Fig. 1C) [15]. The level of stimulus affects only the frequency of bursts, not their amplitude and duration, which implies FM (Fig. 1D and inset) [15, 19]. Similarly, Msn2 and its homologue Msn4 exhibit FM under glucose limitation [10]. Bursty FM is also found in bacteria and mammals, indicating that this is a general modulation scheme across different cell types. For example, during energy-depletion stress, the bacterium *Bacillus subtilis* activates the alternative sigma factor σ^B in discrete stochastic pulses, regulating around 150 downstream genes [20]. In addition, isoform NFAT4 in activated T-cells shows similar behavior [21].

What are the relative benefits of AM and FM? One important issue is the susceptibility to noise, which affects the accuracy of sensing. For example, in broadcasting radio signals it is well known that FM is less affected by noise than AM. This is because noise mainly deteriorates the amplitude, which is where the information is stored in AM. A similar argument also favors action potentials in communicating neuronal signals over long distances [22]. In contrast, it has been hypothesized that for other cell types, such as yeast, the bursty nature of FM may introduce more noise than AM, so that AM might be preferable (Fig. 2A,B) [15]. However, two recent articles (which we discuss below) disagree with this and suggest that FM may still be more accurate [23, 24]. In addition, it is important to remember that there are often other factors than noise minimization. For example, it has been suggested that, in situations where multiple genes need to be up or down regulated, FM can provide greater coordination and reliability (Fig. 2C,D) [15, 19].

Mora and Wingreen considered a model for a single receptor embedded in a cell membrane and compared the noise in the output for two signaling mechanisms: continuous (CM) and bursty (BM) modulation [23]. In CM, the receptor signals continuously whenever a ligand is bound, whereas in BM the receptor signals for a short, fixed-sized burst only upon binding of a ligand. As we explain below, for multiple receptors these mechanisms become equivalent to AM and FM, respectively. By considering integral feedback control, a common network for sensing concentration ramps and precise adaptation [25–27], it was found that, for fast binding and unbinding, the noise in CM can be twice that from BM, suggesting that FM leads to greater accuracy. Despite this unexpected result, there are two key points that need further clarification. First, the response was only calculated to lowest order in the small-ramp parameter, thus neglecting any time dependence of the noise. Second, the derivation solely relied on the small-noise approximation, which might work well for fast signaling, but could be inadequate for slow gene regulation.

Similarly, Tostevin *et al.* found biologically relevant parameter regimes of promoter switching in gene regulation in which an oscillating input can produce a more constant and hence less noisy protein output level than a constant input with noise [24]. Although interesting, this model is restricted to decoding and linear pathways, and requires fine-tuning. Its general applicability remains unclear, such as whether an oscillatory input signal can be replaced by random bursts and still remain more accurate than a constant input. In fact, oscillating signals are well-known to maximize target responsiveness while bypassing desensitization from constant signals [28]. They also globally entrain with its period robust to noise [29]. Such oscillators are found in circadian clocks, segmentation clocks, cell cycle, p53 DNA repair pathways, as well as nuclear factor NF- κ B, epidermal growth factor ERK, cAMP and Ca^{2+} signaling [17, 30–39]. This leaves the question of the relative benefits of AM and FM (with respect to random bursts) largely unanswered.

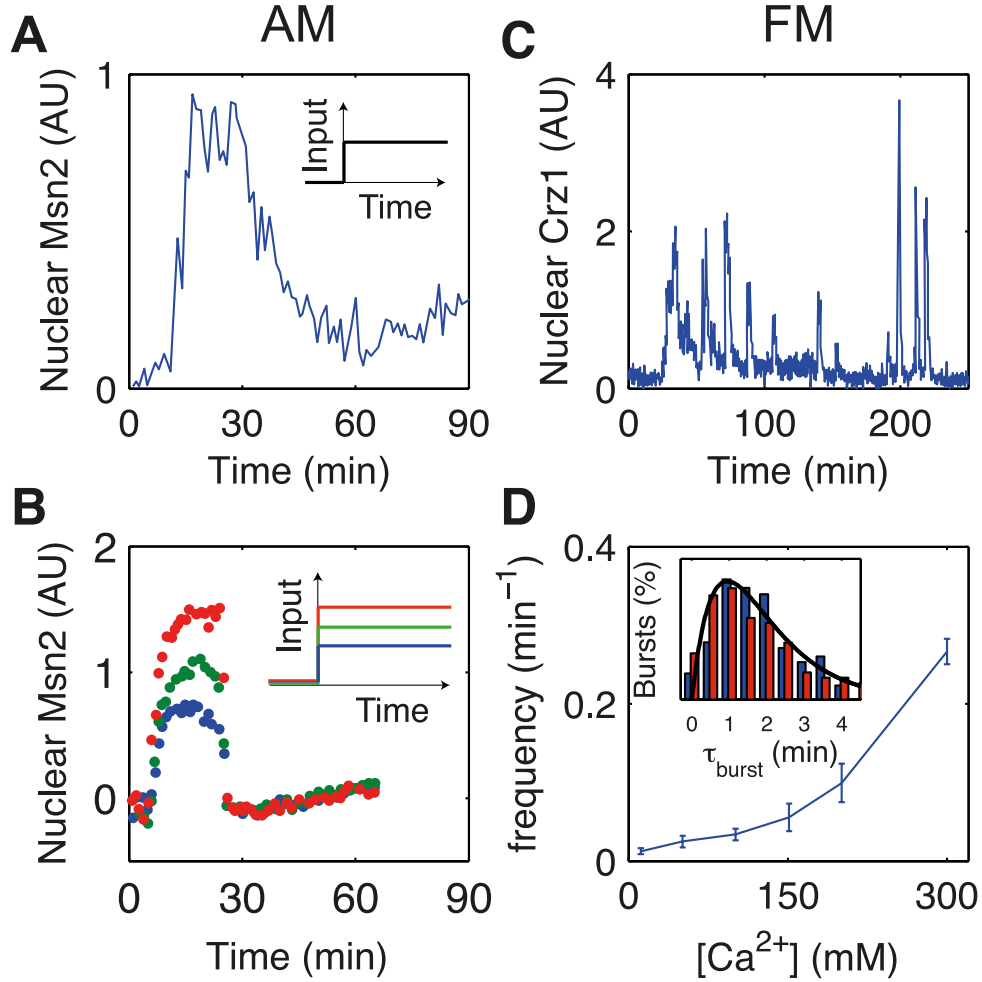


Figure 1. Experimental evidence for amplitude and frequency modulation. (A and B) Example data showing amplitude modulation from [10]. (A) Single-cell nuclear localization of Msn2 transcription factor in response to H_2O_2 stress as a function of time. The stimulus profile (input) is a step change applied at $t = 0$ (inset) which applies to all figure panels. (B) Average time trace for different concentrations of H_2O_2 stress. (C and D) Example data showing frequency modulation from [15]. (C) Single-cell nuclear localization of Crz1 in response to calcium stress as a function of time, showing bursts of Crz1. (D) The average frequency of bursts against calcium concentration, showing an increased frequency with increased concentration. (Inset) Burst duration distribution for low (blue bars) and high (red bars) concentration. Both histograms are well described by the Gamma distribution $h(t) = te^{-t/\tau_b}$, with $\tau_b = 70\text{s}$ (black solid line), demonstrating that pulse duration is independent of calcium concentration. Experimental data in arbitrary units (AU) of fluorescence.

Here, we aim to investigate the advantages and disadvantages of CM and BM (AM and FM) for encoding and decoding of constant concentrations and ramps. To build intuition, we start with a single receptor/ion channel (CM and BM). We consider concentration sensing by a linear pathway, allowing us to gain exact results for different temporal regimes (as suitable for fast signaling and slow gene regulation). To provide analytical results, we extend the single-receptor model for ramp sensing by

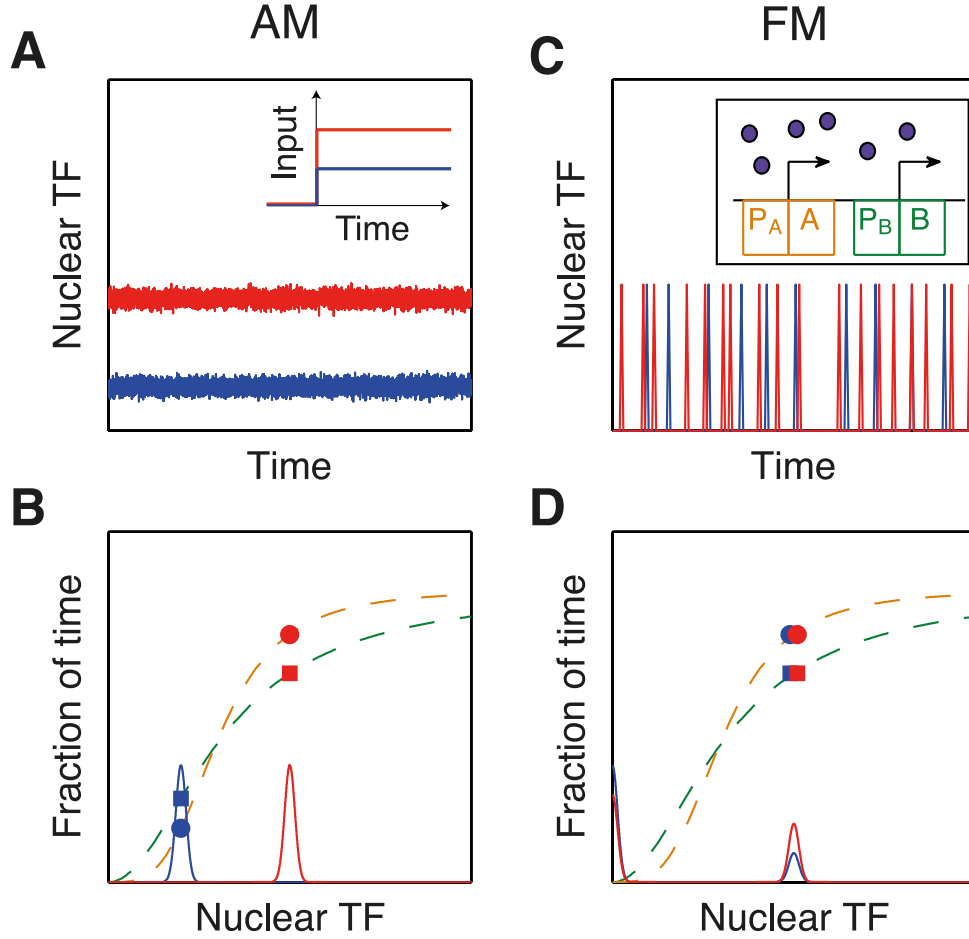


Figure 2. Advantages and disadvantages of amplitude and frequency modulation. AM may be less noisy than FM (A,B), but FM may allow coordinated expression of many genes (C,D) [15, 19]. (A) In AM, low/high stimuli result in low/high levels of transcription factor (TF) inside the nucleus. (B) In AM, different nuclear TF concentrations (blue and red curves) lead to gene expression of proteins A and B (see orange and green promoter functions respectively) with variable ratios (order of dot and square changes). (C) In FM, the stimulus strength only affects the frequency of bursts, not their amplitude. (Inset) Schematic of TF (purple dots) binding promoter P_A of gene A (orange) and promoter P_B of gene B (green) with different binding strengths. (D) In FM, the nuclear TF concentration is always the same during a burst, only the frequency of occurrence changes. As a consequence, the protein ratio stays constant.

Mora and Wingreen. First, we introduce an alternative mechanism to integral feedback, the incoherent feedforward loop (another common pathway motif for ramp sensing and precise adaptation [40–42]). This allows us to generalize the model to more than one pathway. Second, by explicitly including the time-dependence of signaling noise, we are able to provide first-order analytical results for the accuracy of ramp sensing. Taken together, a general principle emerges, favoring BM for fast signaling and CM for slow gene regulation. Finally, we generalize to many receptors and ion channels, a far more realistic situation for biological systems, allowing us to make connection with AM and FM. While we found that

AM is generally more accurate than FM, we speculate why cells may still utilize FM in certain cases of gene regulation.

Results

Cells sense external stimuli with cell-surface receptors and/or ion channels, which ultimately lead to changes in the concentration and dynamics of active transcription factors (TFs) inside the nucleus. Cells control the response at two different levels. Firstly, cell-surface receptors signal to regulate the activity of TFs in the cytoplasm. Secondly, importin and exportin regulate the entry of active TFs into the nucleus, thereby regulating transcription (Fig. 3A). Here, we build a theoretical model that encodes information from an extra-cellular environment in an intra-cellular representation. We distinguish two ways of encoding this information: continuous modulation (CM) and bursty modulation (BM). Once the information is encoded, various proteins can act together to implement a response (decoding), involving regulatory networks. To provide a general analysis for arbitrary noise we first address concentration sensing in a simple linear pathway using the master equation. However, to derive analytical results for ramp sensing and pathways with feedback we apply the small-noise approximation. We finally extend these models to implement amplitude (AM) and frequency modulation (FM) for many receptors or ion channels. Accuracy is assessed by comparing the protein output noise for the different modulation schemes, assuming that the signal is decoded by the average concentration.

Single-receptor/ion-channel model

Following Mora and Wingreen [23] we build a single-receptor model that implements CM and BM. We call the extra-cellular species c , which is encoded intra-cellularly by the signaling rate u . Assuming we are in the fast diffusion regime in which each ligand molecule can bind the receptor only once, the receptor can be in either of two uncorrelated states: *on* when bound and *off* when unbound. This allows the receptor activity, $r(t)$, to be written mathematically as a binary response, which takes value 1 in the *on* state and 0 in the *off* state. The extra-cellular concentration c affects the unbound time intervals τ_u , such that the binding rate is given by $\langle \tau_u \rangle^{-1} = k_+ c(t)$, where k_+ is the binding rate constant. In contrast, the bound time intervals, τ_b , are exponentially distributed random numbers with average $\langle \tau_b \rangle^{-1} = k_-$, where k_- is the unbinding rate constant, which is independent of the extra-cellular stimulus concentration (inset in Fig. 3A). As for ion channels, some are ligand-gated or regulated by receptors, while others are voltage-gated and hence dependent on action potentials [43]. In all these cases the stimulus affects the opening or closing times. In CM downstream proteins are produced with a constant rate α during each *on* time interval, which leads to a signaling rate $u_{\text{CM}} = \alpha r(t)$, while in BM $\zeta = \alpha k_-^{-1}$ molecules are produced instantly at the moment of binding with rate $u_{\text{BM}} = \zeta \sum \delta(t - t_i^+)$, where t_i^+ are the binding times (Fig. 3B). This choice for ζ allows a meaningful comparison of CM and BM as both produce, on average, the same amount of intracellular species.

General approach to concentration sensing exhibits two regimes of accuracy

In order to provide a general result for arbitrary input fluctuations, we write down the chemical master equation. For simplicity, we only consider concentration sensing with $c(t) = c_0$, but the model can also be applied to ramps. Furthermore, we assume a linear pathway in which the receptor/ion channel activity r directly regulates an output species with copy number n (with production rate u and degradation rate γ) (Fig. 3C, left). Since the receptor/ion channel activity is a two-state system (*on/off*), there are two resulting master equations for CM (one for each state) describing the probability of being in the *on* and

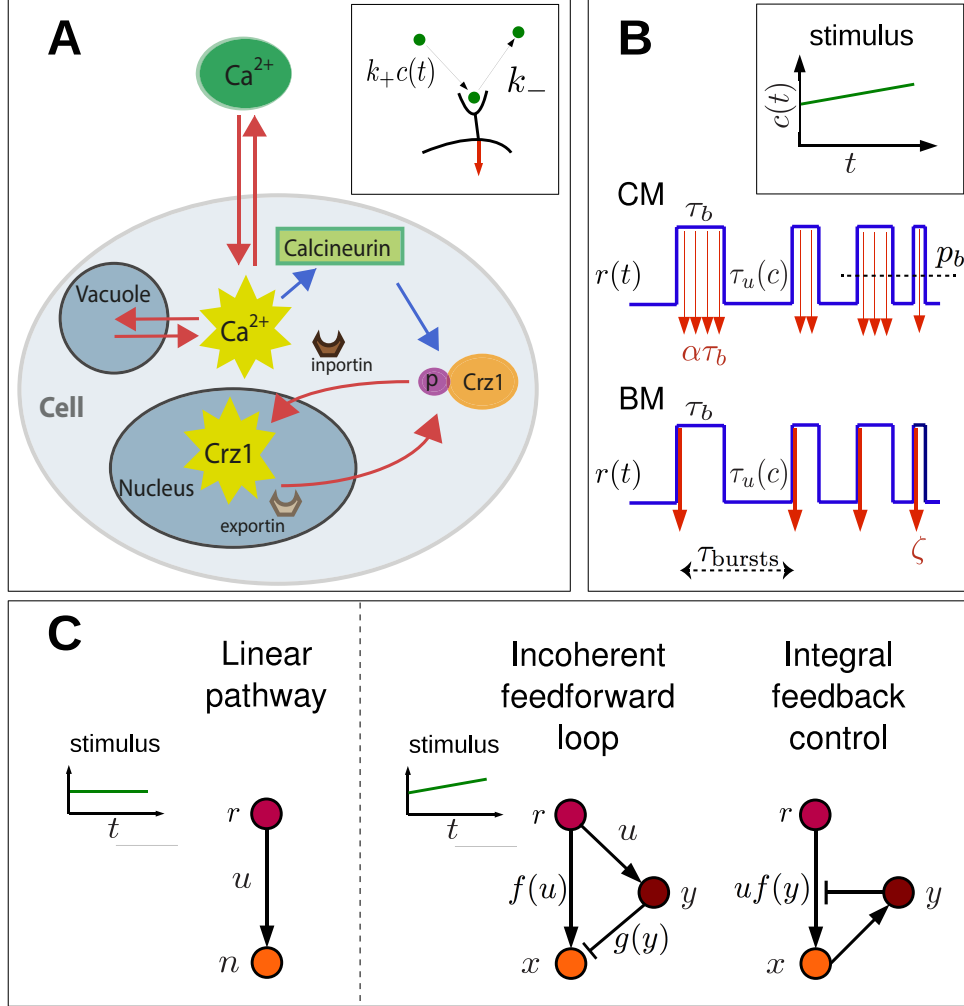


Figure 3. Schematic view of signaling and gene regulation. (A) Cartoon of *S. cerevisiae* in presence of extracellular calcium, considered a paradigm of bursty frequency modulation. Calcium enters through plasma-membrane ion channels and can be stored (released) in (from) vacuoles. Intracellular calcium activates calcineurin, which dephosphorylates Crz1p. Once dephosphorylated, Crz1 binds inporting Nmd5p and enters the nucleus. Exportin Msn5p subsequently removes Crz1 from the nucleus. Cytoplasmic calcium pulses may correspond to Crz1 bursts in the nucleus [15]. Red arrows indicate movement while blue arrows stand for chemical signaling. (B) Single receptor/ion channel activity, $r(t)$ (blue line), depends on the concentration of extra-cellular stimulus c . The signaling rate u differs between continuous (CM) and bursty modulation (BM). In CM, u is constant rate α during bound intervals, with p_b the probability of being bound. In BM, ζ molecules are realized at the time of binding with τ_{bursts} the duration between consecutive bursts (binding events). (C) Different regulatory networks. Linear pathway used for concentration sensing. Incoherent feedforward loop and integral feedback control allow chemical ramps to be sensed.

off states, i.e. $p_{\text{on}}(n, t)$ and $p_{\text{off}}(n, t)$:

$$\frac{dp_{\text{on}}(n, t)}{dt} = \gamma(n+1)p_{\text{on}}(n+1, t) + \alpha p_{\text{on}}(n-1, t) + k_+ c p_{\text{off}}(n, t) - (\gamma n + \alpha + k_-) p_{\text{on}}(n, t), \quad (1a)$$

$$\frac{dp_{\text{off}}(n, t)}{dt} = \gamma(n+1)p_{\text{off}}(n+1, t) + k_- p_{\text{on}}(n, t) - (\gamma n + k_+ c) p_{\text{off}}(n, t). \quad (1b)$$

Note that $\alpha \geq k_-$, so molecules are generally produced in the *on* state. In BM, instead, the master equations which describe the probabilities $p_{on}(n, t)$ and $p_{off}(n, t)$ of having n proteins at time t , are given respectively by

$$\frac{dp_{on}(n, t)}{dt} = \gamma(n+1)p_{on}(n+1, t) + k_+cp_{off}(n-\zeta, t) - (\gamma n + k_-)p_{on}(n, t), \quad (2a)$$

$$\frac{dp_{off}(n, t)}{dt} = \gamma(n+1)p_{off}(n+1, t) + k_-p_{on}(n, t) - (\gamma n + k_+c)p_{off}(n, t), \quad (2b)$$

with burst size ζ a positive integer. We solve Eqs. (1a) and (1b) with generating functions and simulate Eqs. (2a) and (2b) with the Gillespie algorithm (see Materials and Methods).

Simulations via the Gillespie algorithm show different outcomes for fast (small-noise approximation limit, Fig. 4A,B) and slow (Fig. 4C,D) dynamics of the receptor. For fast switching ($k_+c_0, k_- \gg \gamma$), for both CM and BM, the probability has an unimodal distribution (Fig. 4B). On the other hand, in the slow switching regime ($k_+c, k_- \ll \gamma$), the probability distribution becomes bimodal for CM and unimodal with a long tail for BM, leading to drastically increased noise (Fig. 4D). The unimodal distribution for BM, which is simply due to the use of infinitely short pulses, would become bimodal for finite width pulses.

In order to classify the different dynamics and to compare CM and BM for arbitrary noise, we require information on the probability distribution of n output proteins. In particular, we study the average, variance and skewness (the latter is encoded in the third moment) of the distribution for both CM and BM. Constraining the average output of CM and BM to be the same (Fig. 5A,B), we identify two regimes for fast dynamics: $k_+c_0 < k_-$ (Fig. 5C) and $k_+c_0 > k_-$ (Fig. 5D). Specifically, for $k_+c_0 < k_-$, BM is more accurate (Fig. 5C, inset), while CM is generally more accurate when $k_+c_0 > k_-$ (Fig. 5D, inset), except for minimal burst size ($\zeta = 1$). However, for slow dynamics (and hence large noise), CM is always more accurate than BM. The study of the third moment shows that, for slow switching and hence bimodality, BM has large asymmetry (Fig. 5C,F).

These observations can be explained as follows, using the fact that the receptor/ion channel can only detect information from the extra-cellular environment during unbound (*off*) time intervals, as the extra-cellular stimulus only affects the binding rate (Fig. 3). For fast dynamics, the two regimes can be understood by comparison with maximum-likelihood estimation (MLE), the most accurate strategy for encoding [44]. MLE estimates the ligand concentration $c_{ML} = k_+^{-1} \langle \tau_u \rangle^{-1}$ from the average unbound time interval $\langle \tau_u \rangle$. The bound time intervals are discarded as they only contribute noise [44]. BM, which produces fixed-size bursts at the times of binding, approaches MLE when the bound intervals are shorter than the unbound intervals. In this case, the times of the bursts effectively estimate the unbound time intervals (Fig. 3B, bottom) and BM is more accurate than CM. However, when the bound intervals are longer than the unbound intervals, BM cannot estimate the unbound time intervals anymore and becomes less accurate than CM. Since CM produces protein during the bound intervals, it signals according to the average receptor activity $p_b = \langle \tau_b \rangle / (\langle \tau_b \rangle + \langle \tau_u \rangle)$ (Fig. 3B, top). Hence, CM effectively contains information on both bound and unbound intervals, and thus can still provide a reasonable estimate of unbound time intervals. An interesting exception is $\alpha k_-^{-1} = \zeta = 1$, for which BM becomes slightly more accurate than CM. In the latter case, since the rate of protein production during a bound interval in CM is very low, there is uncertainty as to whether CM actually produces protein or not, which reduces its accuracy. In contrast, for slow switching the burst size needs to increase since BM produces the same level of protein as CM. Hence, BM is always less accurate than CM, independent of whether bound or unbound time intervals are longer. While we analytically demonstrate the connection with MLE for fast dynamics in the next section, an extended discussion without comparison to MLE can be found in S1 Text and S1-S3 Figs.

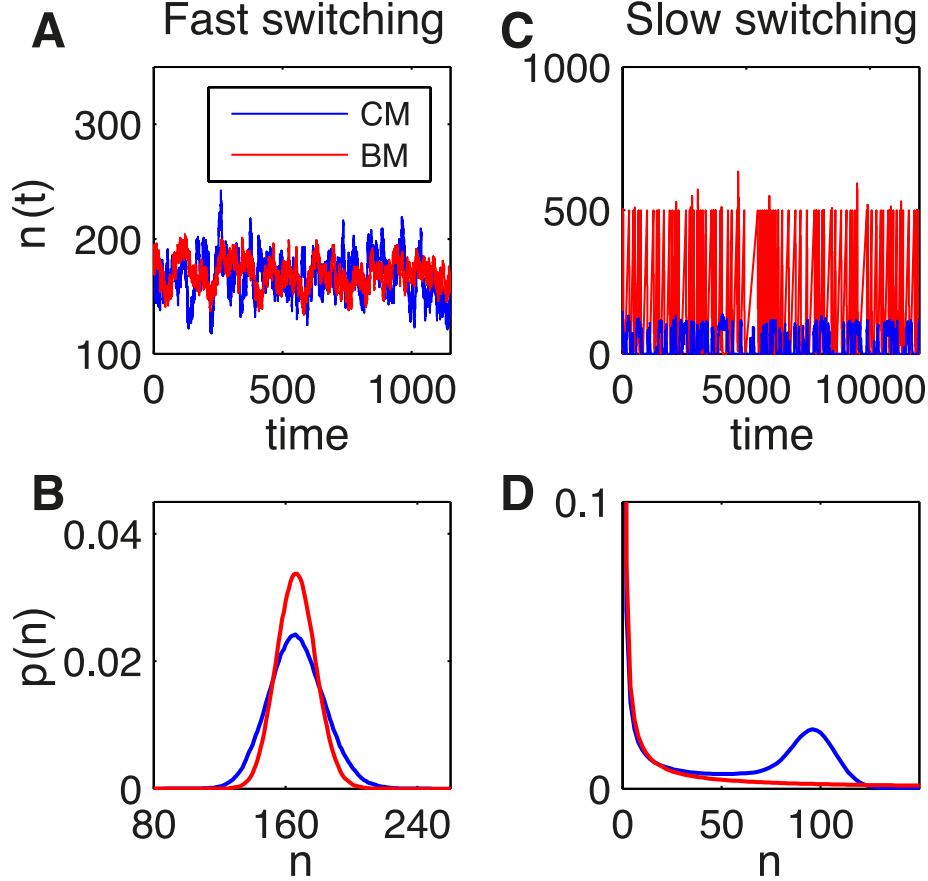


Figure 4. The two regimes in the linear pathway model based on the master equation.

(A-B) fast ($k_+c_0 = 20s^{-1}$, $k_- = 100s^{-1}$, $\gamma = 0.1s^{-1}$, $\alpha = 100s^{-1}$, $\zeta = 1$) and (C-D) slow ($k_+c_0 = 0.01s^{-1}$, $k_- = 0.05s^{-1}$, $\gamma = 1s^{-1}$, $\alpha = 25s^{-1}$, $\zeta = 500$) switching. (A,C) Protein number as a function of time from Gillespie simulations for CM (blue lines) and BM (red lines). (B) The probability distribution for n target proteins is unimodal for both AM (blue) and FM (red). (D) The probability distribution is bimodal for AM (blue) and remains unimodal for BM (red) but with a long tail in the slow switching regime.

Small-noise approximation to ramp sensing confirms two regimes for fast dynamics

To further investigate fast dynamics, we extend an analytical model for ramp sensing in the small-noise approximation [23]. Considering the single-receptor described in Fig. 3A,B, we linearize the system by averaging over a time much larger than the binding and unbinding times. We further assume exponential distributions for τ_b and τ_u so that $\langle(\delta\tau_b)^2\rangle = \langle\tau_b\rangle^2 = k_-^{-2}$ and $\langle(\delta\tau_u)^2\rangle = \langle\tau_u\rangle^2 = (k_+c(t))^{-2}$, where $c(t)$ increases only very slowly with time (see below). Hence, signaling noise arises in CM due to variable bound time intervals (ignoring stochastic production of protein during bound intervals), while in BM the binding times (bursting times) vary. Without loss of generality, we set $\alpha = k_-$, which is equivalent to

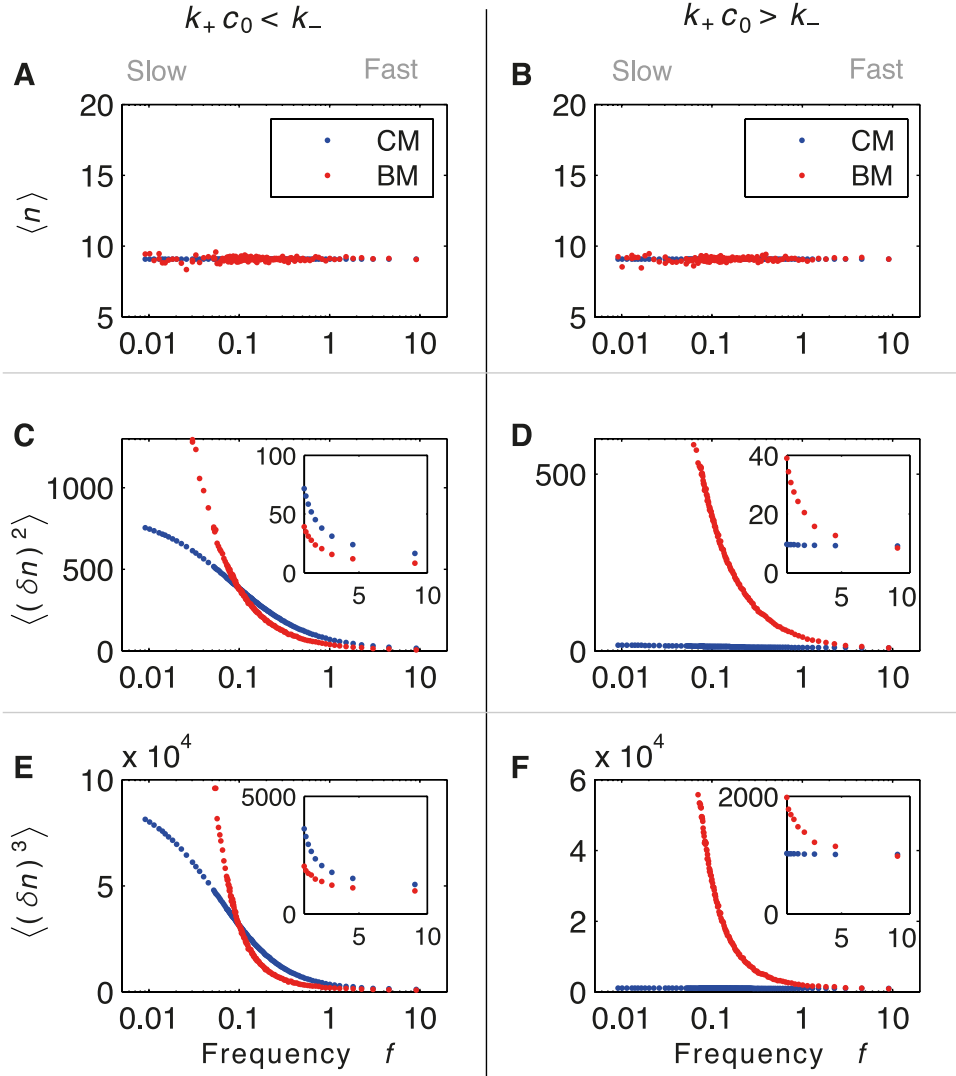


Figure 5. First three moments of the protein distribution in concentration sensing from the master equation. Averages (A,B), variance (C,D), and skewness (E,F) as a function of the frequency of binding events, $f = k_+ c_0 / (1 + k_+ c_0 / k_-)$. (Insets) Magnification of small-noise approximation region (fast switching). Analytical results for CM (blue) and numerical results for BM (red) as function of the frequency of binding events (logarithmic scale). Two regimes are shown: $k_- = 10 k_+ c_0$ ($\alpha = 100 s^{-1}, \gamma = 1 s^{-1}, \zeta$ from 1000 to 1) (left column) and $k_- = 0.1 k_+ c_0$ ($\alpha = 10 s^{-1}, \gamma = 1 s^{-1}, \zeta$ from 1000 to 1) (right column). Averages from CM and BM are constrained to be equal, *i.e.* $\zeta = \alpha k_-^{-1}$. Variances of CM and BM exhibit two different regimes for fast switching: for $k_+ c_0 < k_-$ BM is more accurate than CM (inset in C), while for $k_+ c_0 > k_-$ CM is generally more accurate (inset in D), except for $\zeta = 1$. Third moments show that, for large noise, the probability distributions become asymmetric.

$\zeta = 1$. Hence, as we show in S1 Text, for averaging time much longer than k_-^{-1} and $(k_+ c(t))^{-1}$, the

average and autocorrelation (variance) of $u(t)$ are given by [23]

$$\langle u(t) \rangle = \frac{k_+ c(t)}{1 + k_+ c(t)/k_-}, \quad (3)$$

$$\langle \delta u(t) \delta u(t') \rangle = g \frac{k_+ c(t)}{(1 + k_+ c(t)/k_-)^3} \delta(t - t'), \quad (4)$$

with $\langle \delta u(t) \rangle = 0$ and

$$g = \begin{cases} 1 + \langle (\delta \tau_b)^2 \rangle / \langle \tau_b \rangle^2 & = 2 & \text{CM} \\ 1 + \langle (\delta \tau_b)^2 \rangle / \langle (\delta \tau_u)^2 \rangle & = 1 + [k_+ c(t)/k_-]^2 & \text{BM.} \end{cases} \quad (5)$$

Note that only the variance differs between CM and BM. In particular, in Eq. (5) the ratio $k_+ c(t)/k_-$ determines whether g is larger in BM or CM, which ultimately determines which scheme leads to the least noise. BM has the lower noise only when $k_+ c(t) < k_-$, *i.e.* when $\langle \tau_b \rangle < \langle \tau_u \rangle$. In particular, in the limit of fast unbinding ($k_+ c(t) \ll k_-$), the signaling noise for CM is twice as large as for BM.

Sensing temporal ramps, *i.e.* the change of concentration with time, is crucial for locating nutrients and avoiding toxins. We start by considering a stimulus whose concentration is constant for $t < 0$ and increases linearly and slowly in time after $t = 0$:

$$c(t) = \begin{cases} c_0 & t < 0 \\ c_0 + c_1 t & t \geq 0, \end{cases} \quad (6)$$

for constants c_0 and c_1 with $c_1 t \ll c_0$. By applying Eq. (6) to Eqs. (3-5), the signaling rate can be rewritten to first order as

$$u(t) \simeq \begin{cases} u_0 + u_1 t + \delta u & t \geq 0 \\ u_0 + \delta u & t < 0, \end{cases} \quad (7)$$

where u_0, u_1 are functions of c_0 and c_1 , and δu is the noise described by $\langle \delta u(t) \delta u(t') \rangle$ (given in S1 Text). The condition $c_1 t \ll c_0$ is necessary so that u behaves linearly in time with $u_1 t \ll u_0$. Under this condition, the factor g_{BM} of Eq. (5) becomes

$$g_{\text{BM}} \simeq 1 + \underbrace{\frac{k_+^2 c_0^2}{k_-^2}}_{g_{\text{BM}}^*} + \frac{2k_+^2 c_0 c_1}{k_-^2} t, \quad (8)$$

where g_{BM} is given by g_{BM}^* for a constant external concentration. We now assume that the extra-cellular stimulus is encoded in the signaling rate u which affects the production of two output proteins with concentrations x and y . Specifically, we compare the output noise of x and y between CM and BM using the incoherent feedforward (Fig. 3C, middle) and integral feedback (Fig. 3C, right) loops.

Incoherent feedforward loop

The incoherent feedforward loop is a network motif in which u directly affects two outputs x and y , while y inhibits x (Fig. 3C, middle). The loop provides precise adaptation to a step-change in stimulus and can also be used for ramp sensing. Mathematically, we use the following two coupled stochastic differential equations,

$$\frac{dx}{dt} = k_x \left(\frac{f(u)}{g(y)} - x \right), \quad (9)$$

$$\frac{dy}{dt} = u - k_y y, \quad (10)$$

where k_x is the rate constant for production and degradation of x , while k_y is the rate constant for degradation of y , and $f(u)$ and $g(y)$ are specified functions. In order to have adaptation the variable y needs to evolve slower than x , which requires $k_x > k_y$. Here we choose $f(u) = e^{bu}$ and $g(y) = e^{bk_y y}$, where constant b has units of time. This allows us to obtain an analytic solution (see S1 Text for details).

Integral feedback loop

The integral feedback loop [23] is another network motif for precise adaptation and ramp sensing. Here, u affects x only (the main output), while x activates y and y inhibits x (Fig. 3C, right). The general equations for this model are given by

$$\frac{dx}{dt} = uf(y) - k_x x, \quad (11)$$

$$\frac{dy}{dt} = k_y (x - 1), \quad (12)$$

where k_x is the rate constant for degradation of x , k_y is the rate constant for production and degradation of y satisfying $k_x > k_y$, and $f(y)$ is a monotonically decreasing function of y . Specifically, we choose $f(y) = e^{-by}$, where b is a dimensionless constant. This again produces an analytic solution (see S1 Text for details).

Small-noise approximation

To analytically solve Eqs. (9) and (10) for the incoherent feedforward loop, and Eqs. (11) and (12) for the integral feedback loop, we linearize these equations within the small-noise approximation, and assume that we are in the fast-switching regime. This allows us to find analytic solutions in a particular time window and under certain conditions which we define in S1 Text. Specifically, for the incoherent feedforward loop in the small-ramp regime, the average values of $\langle u(t) \rangle$, $\langle x(t) \rangle$ and $\langle y(t) \rangle$ are determined by the differential equations Eqs. (9,10). Although there are no steady states for ramps, $\langle x(t) \rangle$ and $\langle y(t) \rangle$ show time-dependent stable solutions

$$\langle x(t) \rangle = e^{\frac{bu_1}{k_y}}, \quad (13a)$$

$$\langle y(t) \rangle = \frac{u_0}{k_y} - \frac{u_1}{k_y^2} + \frac{u_1 t}{k_y}. \quad (13b)$$

Introducing $x = \langle x \rangle + \delta x$ and $y = \langle y \rangle + \delta y$ into Eqs. (9) and (10) with subsequent linearization the variance of the target-protein copy numbers can be derived (see Materials and Methods). To first order in small-ramp parameters the variances of x for both types of modulation are

$$\langle (\delta x(t))^2 \rangle_{\text{CM}} = \Delta \left[g_{\text{CM}} u_0 - \frac{1 - 2c_0 k_+ / k_-}{k_x + k_y} u_1 + g_{\text{CM}} (1 - 2k_+ c_0 / k_-) u_1 t \right], \quad (14a)$$

$$\langle (\delta x(t))^2 \rangle_{\text{BM}} = \Delta \left[g_{\text{BM}}^* u_0 - \frac{1 - 2c_0 k_+ / k_- + 3c_0^2 k_+^2 / k_-^2}{2k_y} u_1 + (1 - 2k_+ c_0 / k_- + 3k_+^2 c_0^2 / k_-^2) u_1 t \right], \quad (14b)$$

where $\Delta = \frac{b^2 k_x^2 e^{\frac{2bu_1}{k_y}}}{2(k_x + k_y)(1 + k_+ c_0 / k_-)^2}$, and g_{CM} and g_{BM}^* are parameters discussed in Eqs. (5) and (8). The corresponding results for species y are provided in Eqs. (S56) and (S58), and plots for species x and y are shown in Fig. 6B,D.

Consistent with the master equation, these results show again two regimes: ramp sensing is more accurate for BM if $k_+ c_0 < k_-$, while CM is more accurate otherwise. For a constant environment (zeroth-order with $c_1 = u_1 = 0$) the regime is largely determined by the factor g . If $k_+ c_0 < k_-$,

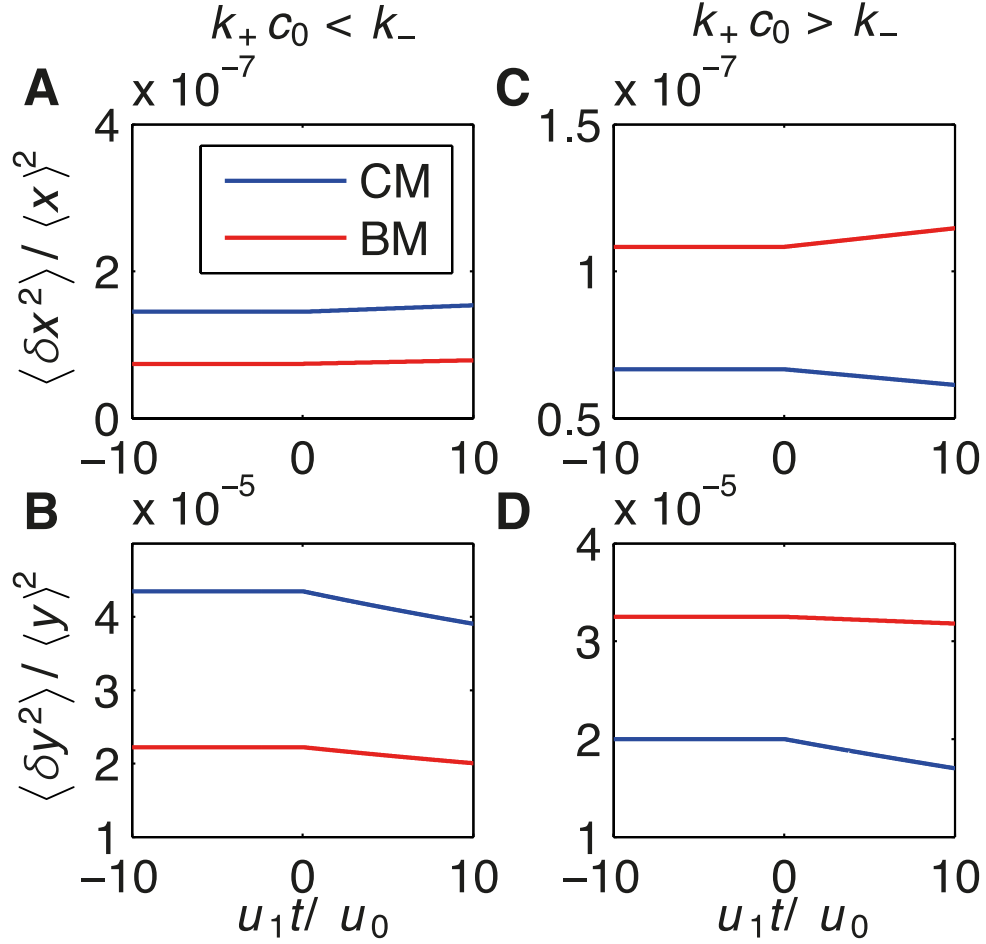


Figure 6. Two regimes in incoherent feedforward loop based on the small-noise approximation. Output noise, *i.e.* relative variance of x (top) and y (bottom), as function of the non-dimensional ramp time $u_1 t / u_0$ for $k_+ c_0 < k_-$ *i.e.* $\langle \tau_b \rangle < \langle \tau_u \rangle$ (left) and $k_+ c_0 > k_-$ *i.e.* $\langle \tau_b \rangle > \langle \tau_u \rangle$ (right). CM and BM are shown by blue and red lines respectively. (A,B) BM is more accurate than AM for $k_+ c_0 = 10^7 s^{-1}$ and $k_- = 6.7 \times 10^7 s^{-1}$. (C,D) CM is more accurate than BM for $k_+ c_0 = 10^7 s^{-1}$ and $k_- = 6.7 \times 10^6 s^{-1}$. Remaining parameters: $k_+ c_1 = 10^5 s^{-2}$, $k_x = 5 s^{-1}$ and $k_y = 10 s^{-1}$.

$g_{BM} = 1 + \langle (\delta \tau_b)^2 \rangle / \langle \delta \tau_u \rangle^2 < 2$ (see Eq. (5)), and BM is more accurate than CM with $g_{CM} = 1 + \langle (\delta \tau_b)^2 \rangle / \langle \tau_b \rangle^2 = 2$ (Fig. 6A,B). This is because the variability of the bound intervals $\langle (\delta \tau_b)^2 \rangle$ can be eliminated in BM (but not in CM), and the unbound intervals are well approximated by the duration between bursts (τ_{bursts} in Fig. 3). For $k_+ c_0 \ll k_-$, BM effectively implements MLE. In contrast, CM is more accurate for $k_+ c_0 > k_-$, where $g_{CM} = 2$ and $g_{BM} > 2$ (Fig. 6C,D). This is because BM contains no information on unbound time intervals, while CM still contains some information through the probability of being bound (p_b in Fig. 3B). These results also apply to ramp sensing since the accuracy of the downstream proteins (decoding) relates again to the factor g and hence to the ratio between the bound and unbound time intervals. The integral feedback loop in Eqs. (11) and (12) shows very similar behavior (provided in S1 Text). The validity of our analytical results are confirmed by simulations of the stochastic differential equation for both pathways in S4 Fig. and S5 Fig.

AM is more accurate than FM for multiple receptors/ion channels

To address the question of whether AM or FM is more accurate in encoding and decoding, we consider a straightforward generalization to multiple receptors (or ion channels) (see S1 Text and S6 Fig. for details). AM can be obtained by considering unsynchronized CM receptors. In contrast, the experimentally observed sporadic bursts of nuclear translocation [10,23] and hence FM might be explained by synchronized receptors that individually operate with BM.

For N unsynchronized (us) receptors, the resulting average and variance of the signaling rate are $\langle u(t) \rangle_N^{us} = N \langle u(t) \rangle_1$ and $\langle \delta u(t) \delta u(t') \rangle_N^{us} = N \langle \delta u(t) \delta u(t') \rangle_1$ in terms of the single-receptor quantities. Consequently, the relative variance, given by the variance divided by the average-squared, scales with the inverse of the number of receptors (N). On the other hand, for N synchronized (s) receptors, the average and variance of the signaling rate are given respectively by $\langle u(t) \rangle_N^s = N \langle u(t) \rangle_1$ and $\langle \delta u(t) \delta u(t') \rangle_N^s = N^2 \langle \delta u(t) \delta u(t') \rangle_1$. The relative variance is now independent of N . Hence, unsynchronized receptors (AM) have a reduction of noise by a factor N compared to synchronized receptors (FM).

For slow dynamics, or fast dynamics with $k_{+c} > k_-$, CM is generally more accurate than BM (at least for $\zeta > 1$), and with N receptors, AM is more accurate than FM by an even larger margin. In contrast, for fast dynamics with $k_{+c} < k_-$, BM is more accurate than CM by at most a factor of 2 (Eq. (5)). But since AM is N times more accurate than CM, AM becomes more accurate for encoding than FM for more than two receptors. Since our results from the previous sections show that larger signaling noise leads to larger output noise, the same rule emerges for decoding.

From a physical point of view, how can receptors act in a synchronized fashion? Receptors may be coupled by adaptor proteins or elastic membrane deformations, allowing them to act cooperatively [45,46]. In conclusion, while for fast dynamics (small-noise approximation) BM can be more accurate than CM up to a factor of two, two receptors/ion channels are sufficient for AM to become more accurate than FM. Since cells have thousands of receptors and ion channels, AM becomes the most accurate modulation scheme.

Discussion

Cellular responses to extra-cellular stimuli involve both encoding the external stimuli by internal signals (which is normally fast) and subsequently decoding via the regulation of protein levels (which is normally much slower). The internal representation of the external signal falls into two broad categories: continuous/amplitude modulation (CM/AM), where bound receptors continually signal and the internal concentration itself encodes the external signal, and bursty/frequency modulation (BM/FM), where receptors only signal when first bound and the signal is encoded in the frequency of peaks. Here, we compared the output noise for both types of modulation in the presence of a constant and a linearly increasing (in time) external concentration. Besides considering a linear pathway, we compared two non-linear network motifs: the incoherent feedforward loop and the integral feedback loop. These loops are ubiquitous in biological systems. For example, the incoherent feedforward loop is found in chemotactic adaptation of eukaryotes [40] and transcription networks in bacteria [41], and the integral feedback loop is found in chemotactic adaptation of bacteria [25,47] and in eukaryotic olfactory and phototransduction pathways [27].

We found that, for a single receptor or ion channel, BM can be more accurate than CM for fast dynamics. This situation can occur when the average duration of the active *on* state is shorter than the average duration of the inactive *off* state (Figs. 5 and 6). In this case, BM effectively implements maximum-likelihood estimation, the most accurate mechanism of sensing [44]. If instead more time is

spent in the *on* state, then CM is generally more accurate (except when the burst size is minimal, i.e. one). The reason behind this effect, which we analytically prove within the small-noise approximation, is that CM has information about both the *on* and *off* states, whereas BM only knows when a switch from *off* to *on* occurs. As such, CM effectively implements Berg and Purcell’s classic result of estimating ligand concentration by time averaging [48] (see also Discussion in [44]). In addition, we found that for slow dynamics CM is always more accurate than BM, independent of whether more time is spent in the *on* or *off* states, due to increased burst sizes (Fig. 5). Taken together our results suggest that BM should be more common in signaling pathways than in gene regulation.

The generalization to multiple receptors/ion channels allows AM and FM to be compared. AM, which arises from unsynchronized CM receptors, has a reduced relative noise due to spatial averaging, while the relative noise in FM from synchronized BM receptors remains identical to the single-receptor result. (Note the observed nuclear bursts of approximately constant amplitude and duration support our FM mechanism [10, 15].) As a result, AM is always more accurate than FM for more than two receptors (S6 Fig.). Since cells have tens of thousands of receptors and ion channels, this implies that the reason that FM is sometimes observed in real systems must have a different origin. At least three possibilities present themselves. Firstly, FM can help to coordinate gene expression [15, 19], which is particularly useful when hundreds of genes are controlled by a single transcription factor, such as during stress response [49–51]. Secondly, FM can enhance co-localization of proteins inside the nucleus, providing another way to improve coordination of gene expression [52]. Thirdly, as with oscillatory signals, bursts can be used to activate transcription by threshold crossing [32] while avoiding desensitization [28]. This may then push the cell to differentiate into a new state (such as under starvation to initiate competence) [53, 54]. It is also worth noting that by using seemingly redundant isoforms (such as NFAT1 and NFAT4 during an immune response), AM and FM can be combined to enhance temporal information processing [21].

While providing intuitive insights, it is clear that our models are highly oversimplified versions of signaling and gene regulation in actual cells. One of the main reasons for this is that we used idealized delta-functions as pulses in BM (and hence in FM). However, for example, in the calcium stress-response pathway in *Saccharomyces cerevisiae* (Fig. 3A) nuclear bursts of Crz1p are on average two minutes long (Fig. 1D, inset). Most likely cytoplasmic calcium spikes determine the nuclear bursts (Elowitz, personal communication), but since the mechanism of calcium spiking remains poorly understood, such bursts are difficult to model. A further limitation of our models is that bursts only relate to translocation, whereas additional bursts may occur further downstream during transcription [55] (e.g. due to promoter switching [24]) and translation [56]. Future models may need to include these details.

Our models suggest further experimental investigation in multiple areas. Firstly, the distribution of burst duration affects factor g (Eq. (5)), so that $g = 2$ in equilibrium for a single-step process and potentially $g < 2$ for an irreversible binding cycle dominated by energy dissipation [23, 57]. These irreversible cycles are present in some ligand-gated ion channels, such as the cystic fibrosis transmembrane conductance regulator (CFTR) channels and N-Methyl-D-aspartate (NMDA) receptors. These exhibit peaked opening distributions, which can be interpreted as evidence of broken reversibility and energy consumption [58, 59]. Such cases and their possible connection with accuracy need further investigation. In fact, most cellular processes rely heavily on energy consumption, including nuclear shuttling and chromosome remodeling, limiting the applicability of our equilibrium CM-receptor model. Secondly, coordination of gene expression during stress or cell-fate decisions might be another reason for implementing FM rather than AM. More quantitative experiments are needed to better understand this mechanism. Thirdly, closer inspection of Ca^{2+} -independent transcription factors (as well as Ca^{2+} -dependent co-regulated genes) are warranted in order to verify coordination of multiple genes [15]. Finally, to see if bursts help jump start new cellular programs (*i.e.* transition into a new “attractor”), global changes in gene regulation can be monitored.

A general understanding of FM may help prevent developmental defects and human diseases. Indeed, several biomedically relevant transcription factors, such as NF- κ B, p53, NFAT and ERK, show oscillatory

pulsing or random bursting [16,17,33–36,54]. In fact, the destabilization of regulatory circuits can underlie human diseases: studies suggest that the coordination of gene expression could be critical in maintaining the proper functioning of key nodes in such circuits. For example, the NFATc circuit is cooperatively destabilized by a 1.5-fold increase in the DSCR1 and DYRK1A genes, which reduce NFATc activity leading to characteristics of Down’s syndrome [16,60]. However, ERK pulses are regulated by both AM and FM with the same dose dependence, and it remains unclear how they affect cell proliferation and the relevance to cancer [36].

Broadly speaking, temporal ordering (regularity or periodicity) serves at least two roles in living systems [61]: extraction of energy from the environment and handling of information. While the first role is well studied in terms of molecular motors at the single-molecule level, the second role is intellectually more difficult to understand as it requires a broader, more global understanding of cells. We believe that future work that combines single-cell experiments with ideas of collective behavior and engineering principles is most likely to be successful.

Materials and Methods

Master-equation model for concentration sensing

The master equations for continuous modulation (CM), Eqs. (1a) and (1b), can be solved at steady state using generating functions. In particular, we derive the first three moments of the probability distribution using the general model in [62]. When the system is in the *on/off* state, the production rate of species x is $\alpha_{on/off}$. The degradation rate γ is independent of the state of the system. The probability distribution of n target proteins at time t is then described by

$$\frac{dp_s(n, t)}{dt} = \gamma(n+1)p_s(n+1, t) + \alpha_s p_s(n-1, t) + k_{\bar{s}} p_{\bar{s}}(n, t) - (\gamma n + \alpha_s + k_s) p_s(n, t), \quad (15)$$

where $\bar{s} = \text{off}$ (on) when $s = \text{on}$ (off). By defining the generating functions

$$G_s(z) = \sum_{n=0}^{\infty} p_s(n) z^n, \quad (16)$$

and using Eq. (15), a solution for $G_s(z)$ can be found, which then readily gives the moments of $p(n, t)$. In particular, the variance and skewness are given by

$$\langle \delta n^2 \rangle = \sum_s (\partial_z z \partial_z G_s(z)) \Big|_{z=1} - \langle n \rangle^2, \quad (17)$$

$$\langle n^3 \rangle = \sum_s [\partial_z z \partial_z z \partial_z G_s(z)] \Big|_{z=1}. \quad (18)$$

Full details are given in S1 Text.

In order to solve the master equation for bursty modulation (BM), Eqs. (2a) and (2b), we use the Gillespie algorithm [63]. If the system is in the *on* state with n proteins at time t , it can either switch to the *off* state with transition rate given by $k_-/(k_- + \gamma n)$ or else remain in the *on* state and lose a protein by degradation. If instead the system is in the *off* state with n proteins at time t , it can either switch to the *on* state with switching rate $k_+ c_0/(k_+ c_0 + \gamma n)$ and, via a burst, increase its number of proteins to $n + \zeta$, or again remain in the same state and loose a protein by degradation. The time step between reactions, δt , is chosen from an exponential probability distribution $\lambda e^{-\lambda \delta t}$, with λ equal to the total rate that at least one reaction occurs.

ODE models for ramp sensing

The following method applies to both the incoherent feedforward and the integral feedback loop. To solve the ordinary differential equations (9-12) we linearize around stable solutions, $x(t) = \langle x(t) \rangle + \delta x$ and $y(t) = \langle y(t) \rangle + \delta y$, and assume that small δu leads to small δx and δy . Note that when sensing a gradually changing ramp, $\langle x(t) \rangle$ and $\langle y(t) \rangle$ are not steady states. Defining $X = [x(t) \ y(t)]^T$ we can rewrite these equations as

$$\frac{dX(t)}{dt} + MX(t) = \begin{bmatrix} w \ \delta u \\ z \ \delta u \end{bmatrix}, \quad (19)$$

where the matrix M and the constants w and z are defined in S1 Text. Analytic solutions are only available when M is time-independent. As shown in S1 Text, Eq. (19) can be solved and written as an integral, which can then be evaluated with, for example, Wolfram Mathematica 8.

Acknowledgments

We thank Guido Tiana for helpful discussions, and Michael Elowitz for providing details on his data. GM and RGE acknowledge funding from ERC Starting-Grant N. 280492-PPHPI. GA was supported by Leverhulme-Trust grant N. RPG-181 and DMR was supported by BBSRC grant N. P34460.

References

1. Perkins TJ, Swain PS. Strategies for cellular decision-making. *Mol Syst Biol.* 2009 Nov;5:326.
2. Kussell E, Leibler S. Phenotypic diversity, population growth, and information in fluctuating environments. *Science.* 2005 Sep;309(5743):2075–2078.
3. Behar M, Hoffmann A. Understanding the temporal codes of intra-cellular signals. *Curr Opin Genet Dev.* 2010 Dec;20(6):684–693.
4. Black JW, Leff P. Operational models of pharmacological agonism. *Proc R Soc Lond B Biol Sci.* 1983 Dec;220(1219):141–162.
5. Mackeigan JP, Murphy LO, Dimitri CA, Blenis J. Graded mitogen-activated protein kinase activity precedes switch-like c-Fos induction in mammalian cells. *Mol Cell Biol.* 2005 Jun;25(11):4676–4682.
6. Yu RC, Pesce CG, Colman-Lerner A, Lok L, Pincus D, Serra E, et al. Negative feedback that improves information transmission in yeast signalling. *Nature.* 2008 Dec;456(7223):755–761.
7. Bosisio D, Marazzi I, Agresti A, Shimizu N, Bianchi ME, Natoli G. A hyper-dynamic equilibrium between promoter-bound and nucleoplasmic dimers controls NF- κ B-dependent gene activity. *EMBO J.* 2006 Feb;25(4):798–810.
8. Werner SL, Kearns JD, Zadorozhnaya V, Lynch C, O’Dea E, Boldin MP, et al. Encoding NF- κ B temporal control in response to TNF: distinct roles for the negative regulators I κ B α and A20. *Genes Dev.* 2008 Aug;22(15):2093–2101.
9. Giorgetti L, Siggers T, Tiana G, Caprara G, Notarbartolo S, Corona T, et al. Noncooperative interactions between transcription factors and clustered DNA binding sites enable graded transcriptional responses to environmental inputs. *Mol Cell.* 2010 Feb;37(3):418–428.
10. Hao N, O’Shea EK. Signal-dependent dynamics of transcription factor translocation controls gene expression. *Nat Struct Mol Biol.* 2012 Jan;19(1):31–39.

11. Paszek P, Jackson DA, White MR. Oscillatory control of signalling molecules. *Curr Opin Genet Dev.* 2010 Dec;20(6):670–676.
12. D’Andrea P, Codazzi F, Zacchetti D, Meldolesi J, Grohovaz F. Oscillations of cytosolic calcium in rat chromaffin cells: dual modulation in frequency and amplitude. *Biochem Biophys Res Commun.* 1994 Dec;205(2):1264–1269.
13. Berridge MJ. The AM and FM of calcium signalling. *Nature.* 1997 Apr;386:759–760.
14. Berridge MJ, Galione A. Cytosolic calcium oscillators. *FASEB J.* 1988 Dec;2(15):3074–3082.
15. Cai L, Dalal CK, Elowitz MB. Frequency-modulated nuclear localization bursts coordinate gene regulation. *Nature.* 2008 Sep;455(7212):485–490.
16. Crabtree GR, Graef IA. Bursting into the nucleus. *Sci Signal.* 2008 Dec;1(51):pe54.
17. Levine JH, Lin Y, Elowitz MB. Functional roles of pulsing in genetic circuits. *Science.* 2013 Dec;342(6163):1193–1200.
18. Connor FR. Introductory topics in electronics and telecommunication: modulation. The Universities Press, Belfast; 1973.
19. Eldar A, Elowitz MB. Functional roles for noise in genetic circuits. *Nature.* 2010 Sep;467(7312):167–173.
20. Locke JC, Young JW, Fontes M, Hernández Jiménez MJ, Elowitz MB. Stochastic pulse regulation in bacterial stress response. *Science.* 2011 Oct;334(6054):366–369.
21. Yissachar N, Sharar Fischler T, Cohen AA, Reich-Zeliger S, Russ D, Shifrut E, et al. Dynamic response diversity of NFAT isoforms in individual living cells. *Mol Cell.* 2013 Jan;49(2):322–330.
22. Lisman JE. Bursts as a unit of neural information: making unreliable synapses reliable. *Trends Neurosci.* 1997 Jan;20(1):38–43.
23. Mora T, Wingreen NS. Limits of sensing temporal concentration changes by single cells. *Phys Rev Lett.* 2010 Jun;104(24):248101–248101.
24. Tostevin F, de Ronde W, ten Wolde PR. Reliability of frequency and amplitude decoding in gene regulation. *Phys Rev Lett.* 2012 Mar;108(10):108104–108104.
25. Yi TM, Huang Y, Simon MI, Doyle J. Robust perfect adaptation in bacterial chemotaxis through integral feedback control. *Proc Natl Acad Sci U S A.* 2000 Apr;97(9):4649–4653.
26. Barkai N, Leibler S. Robustness in simple biochemical networks. *Nature.* 1997 Jun;387(6636):913–917.
27. De Palo G, Facchetti G, Mazzolini M, Menini A, Torre V, Altafini C. Common dynamical features of sensory adaptation in photoreceptors and olfactory sensory neurons. *Sci Rep.* 2013 Feb;3:1251.
28. Li Y, Goldbeter A. Pulsatile signaling in intercellular communication. Periodic stimuli are more efficient than random or chaotic signals in a model based on receptor desensitization. *Biophys J.* 1992 Jan;61(1):161–171.
29. Rapp PE, Mees AI, Sparrow CT. Frequency encoded biochemical regulation is more accurate than amplitude dependent control. *J Theor Biol.* 1981 Jun;90(4):531–544.

30. Tyson JJ, Novak B. Cell cycle: who turns the crank? *Curr Biol.* 2011 Mar;21(5):185–187.
31. McWatters H, Dunlap JC, Millar AJ. Circadian biology: clocks for the real world. *Curr Biol.* 1999 Sep;9(17):633–635.
32. Dolmetsch RE, Xu K, Lewis RS. Calcium oscillations increase the efficiency and specificity of gene expression. *Nature.* 1998 Apr;392(6679):933–936.
33. Batchelor E, Loewer A, Mock C, Lahav G. Stimulus-dependent dynamics of p53 in single cells. *Mol Syst Biol.* 2011 May;7:488–488.
34. Ashall L, Horton CA, Nelson DE, Paszek P, Harper CV, Sillitoe K, et al. Pulsatile stimulation determines timing and specificity of NF- κ B-dependent transcription. *Science.* 2009 Apr;324(5924):242–246.
35. Tay S, Hughey JJ, Lee TK, Lipniacki T, Quake SR, Covert MW. Single-cell NF- κ B dynamics reveal digital activation and analogue information processing. *Nature.* 2010 Jul;466(7303):267–271.
36. Albeck JG, Mills GB, Brugge JS. Frequency-modulated pulses of ERK activity transmit quantitative proliferation signals. *Mol Cell.* 2013 Jan;49(2):249–261.
37. Cai H, Katoh-Kurasawa M, Muramoto T, Santhanam B, Long Y, Li L, et al. Nucleocytoplasmic shuttling of a GATA transcription factor functions as a development timer. *Science (New York, NY).* 2014 Mar;343(6177):1249531.
38. Gregor T, Fujimoto K, Masaki N, Sawai S. The onset of collective behavior in social amoebae. *Science.* 2010 May;328(5981):1021–1025.
39. Goldbeter A, Gérard C, Gonze D, Leloup JC, Dupont G. Systems biology of cellular rhythms. *FEBS Lett.* 2012 Aug;586(18):2955–2965.
40. Takeda K, Shao D, Adler M, Charest PG, Loomis WF, Levine H, et al. Incoherent feedforward control governs adaptation of activated ras in a eukaryotic chemotaxis pathway. *Sci Signal.* 2012 Jan;5(205).
41. Shen-Orr SS, Milo R, Mangan S, Alon U. Network motifs in the transcriptional regulation network of *Escherichia coli*. *Nat Genet.* 2002 May;31(1):64–68.
42. Goentoro L, Shoal O, Kirschner MW, Alon U. The incoherent feedforward loop can provide fold-change detection in gene regulation. *Mol Cell.* 2009 Dec;36(5):894–899.
43. Hille B. Ion channels of excitable membranes. 3rd ed. Sinauer Associates Inc 2001-07; 2001.
44. Endres RG, Wingreen NS. Maximum likelihood and the single receptor. *Phys Rev Lett.* 2009 Oct;103(15):158101–158101.
45. Endres RG. Polar chemoreceptor clustering by coupled trimers of dimers. *Biophys J.* 2009 Jan;96(2):453–463.
46. Wiggins P, Phillips R. Membrane-protein interactions in mechanosensitive channels. *Biophys J.* 2005 Feb;88(2):880–902.
47. Alon U, Surette MG, Barkai N, Leibler S. Robustness in bacterial chemotaxis. *Nature.* 1999 Jan;397(6715):168–171.
48. Berg H, Purcell E. Physics of chemoreception. *Biophysical Journal.* 1977 Nov;20(2):193–219.

49. Yoshimoto H, Saltsman K, Gasch AP, Li HX, Ogawa N, Botstein D, et al. Genome-wide analysis of gene expression regulated by the calcineurin/Crz1p signaling pathway in *Saccharomyces cerevisiae*. *J Biol Chem*. 2002 Aug;277(34):31079–31088.
50. Hoffmann A, Baltimore D. Circuitry of nuclear factor κ B signaling. *Immunol Rev*. 2006 Apr;210:171–186.
51. Schmitt AP, McEntee K. Msn2p, a zinc finger DNA-binding protein, is the transcriptional activator of the multistress response in *Saccharomyces cerevisiae*. *Proc Natl Acad Sci U S A*. 1996 Jun;93(12):5777–5782.
52. Kang J, Xu B, Yao Y, Lin W, Hennessy C, Fraser P, et al. A dynamical model reveals gene co-localizations in nucleus. *PLoS Comput Biol*. 2011 Jul;7(7).
53. Ferrell JE. Bistability, bifurcations, and Waddington’s epigenetic landscape. *Curr Biol*. 2012 Jun;22(11):458–466.
54. Purvis JE, Karhohs KW, Mock C, Batchelor E, Loewer A, G L. p53 dynamics control cell fate. *Science*. 2012 Jun;336:1440–1444.
55. Muramoto T, Cannon D, Gierlinski M, Corrigan A, Barton GJ, Chubb JR. Live imaging of nascent RNA dynamics reveals distinct types of transcriptional pulse regulation. *Proc Natl Acad Sci U S A*. 2012 May;109(19):7350–7355.
56. Thattai M, van Oudenaarden A. Intrinsic noise in gene regulatory networks. *Proc Natl Acad Sci U S A*. 2001 Jul;98(15):8614–8619.
57. Lang AH, Fisher CK, Mora T, Mehta P. Thermodynamics of statistical inference by cells. *Phys Rev Lett*. 2014 Oct;113(14):148103–148103.
58. Csanády L, Vergani P, Gadsby DC. Strict coupling between CFTR’s catalytic cycle and gating of its Cl⁻ ion pore revealed by distributions of open channel burst durations. *Proc Natl Acad Sci U S A*. 2010 Jan;107(3):1241–1246.
59. Schneggenburger R, Ascher P. Coupling of permeation and gating in an NMDA-channel pore mutant. *Neuron*. 1997 Jan;18(1):167–177.
60. Arron JR, Winslow MM, Polleri A, Chang CP, Wu H, Gao X, et al. NFAT dysregulation by increased dosage of DSCR1 and DYRK1A on chromosome 21. *Nature*. 2006 Jun;441(7093):595–600.
61. Anderson PW. More is different. *Science*. 1972 Aug;177(4044):393–6.
62. Mehta P, Schwab DJ. Energetic costs of cellular computation. *Proc Natl Acad Sci U S A*. 2012 Oct;109(44):17978–17982.
63. Gillespie DT. A general method for numerically simulating the stochastic time evolution of coupled chemical reactions. *J Comput Phys*. 1976;22(4):403 – 434.

Supporting Information Legends

S1 Text. Details of analytical calculations.

S1 Fig. First three moments of the protein distribution in concentration sensing from the master equation. Averages (A,B), variance (C,D), and skewness (E,F) as a function of the frequency of binding events, $f = k_+c_0/(1 + k_+c_0/k_-)$. (Insets) Magnification of small-noise approximation region (fast switching). Analytical results for CM (blue) and numerical results for BM (red) and intermediate modulation IM (green) as function of the frequency of binding events (logarithmic scale). Note that this figure is similar to Fig. 5 in main text with the addition of IM. Two regimes are shown: $k_- = 10 k_+c_0$ ($\alpha = 100s^{-1}, \gamma = 1s^{-1}, \zeta$ from 1000 to 1) (left column) and $k_- = 0.1 k_+c_0$ ($\alpha = 10s^{-1}, \gamma = 1s^{-1}, \zeta$ from 1000 to 1) (right column). Averages from CM, BM and IM are constrained to be equal, *i.e.* ζ (BM) = αk_-^{-1} (CM) = $\alpha' \tau_b$ (IM). Variances of CM, BM and IM exhibit two different regimes for fast switching: for $k_+c_0 < k_-$ BM is the most accurate mechanism and CM the worst (inset in C) while for $k_+c_0 > k_-$ CM is generally the most accurate (except for $\zeta = 1$) and IM the worst (inset in D). Third moments show that, for large noise, the probability distributions become asymmetric.

S2 Fig. Examples of time traces of receptor activity and protein copy numbers for different regimes. (Top) Regime $k_+c_0 < k_-$ with $k_+c = 0.1 k_-$ ($\alpha = 100s^{-1}, \gamma = 1s^{-1}$). (Bottom) Regime $k_+c_0 > k_-$ with $k_+c = 10 k_-$ ($\alpha = 10s^{-1}, \gamma = 1s^{-1}$). (Left) Slow switching with $\zeta = 400$. (Right) Fast switching with $\zeta = 7$. Receptor activity r and protein copy numbers $n(t)$ for CM, BM and IM are shown in black, blue, red and green, respectively.

S3 Fig. Investigating accuracy based on accumulative signaling (without protein production and degradation). (A) Regime $k_+c_0 < k_-$ with $k_+c = 0.1 k_-$ ($\alpha = 100s^{-1}, \gamma = 1s^{-1}$ and $\zeta = 7$). (Left) ODE model. (Right) Stochastic protein production during τ_b in CM and IM. (Top) Examples of time traces. (Bottom) Histograms of number of proteins produced after 100s with standard deviation in legend based on 1000 simulations. (B) Analogous to (A) but for regime $k_+c > k_-$ with $k_+c = 10 k_-$ ($\alpha = 100s^{-1}, \gamma = 1s^{-1}$ and $\zeta = 7$). CM, BM and IM are shown in blue, red and green, respectively.

S4 Fig. Incoherent feedforward loop: Comparison of analytical results with simulations of the stochastic differential equations. (A) Averages of signaling rate u (left), species y from Eq. (S42) (middle) and species x from (S41) (right) as a function of time. Analytic solutions Eqs. (S32), (S43) and (12) are shown for BM in red, while a (time averaged) time-trace from a stochastic simulation using the Euler method is shown in orange (CM is almost identical and hence is not shown). (B) Corresponding variances as a function of time for $k_+c_0 > k_-$ ($k_- = 6.7 \times 10^5 s^{-1}$, $k_+c_0 = 10^6 s^{-1}$). Analytic results are shown in blue for CM and in red for BM; average over time (1s) from numerical simulations are shown in light blue for CM and in orange for BM. (C) Corresponding variances as a function of time for $k_+c_0 < k_-$ ($k_- = 6.7 \times 10^6 s^{-1}$, $k_+c_0 = 10^6 s^{-1}$). Colors same as in (B). Remaining parameters: $k_+c_1 = 10^4 s^{-2}$, $k_x = 10 s^{-1}$ and $k_y = 50 s^{-1}$.

S5 Fig. Integral feedback loop: Comparison of analytical results with simulations of the stochastic differential equations. (A) Averages of signaling rate u (left), species y from Eq. (S60) (middle) and species x from (S59) (right) as a function of time. Analytic solutions Eqs. (S32), (S66) and (S65) are shown for BM in red, while a (time averaged) time-trace from a stochastic simulation using the Euler method is shown in orange (CM is almost identical and hence is not shown). (B) Corresponding variances as a function of time for $k_+c_0 > k_-$ ($k_- = 6.7 \times 10^5 s^{-1}$, $k_+c_0 = 10^6 s^{-1}$). Analytic results are shown in blue for CM and in red for BM; numerical simulations are shown in light blue for CM and in orange for BM. (C) Corresponding variances as a function of time for $k_+c_0 < k_-$ ($k_- = 6.7 \times 10^6 s^{-1}$, $k_+c_0 = 10^6 s^{-1}$). Colors same as in (B). Remaining parameters: $k_+c_1 = 10^4 s^{-2}$, $k_x = 10 s^{-1}$ and $k_y = 50 s^{-1}$.

S6 Fig. From CM (BM) to AM (FM) for multiple receptors/ion channels. (A-D) Schematic of receptor activity in time. (A) AM emerges from N unsynchronized receptors or ion channels in CM mode. (B) N synchronized CM receptors lead to a hybrid mechanism with information encoded in the frequency of broad bursts of variable duration. (C) N unsynchronized BM receptors provide a dense series of bursts. For large N , bursts may start overlapping, leading to variable amplitudes. (D) FM emerges from N synchronized receptors in BM mode. (E) Relative variance for a system of 8 receptors with ρN synchronized and $(1 - \rho)N$ unsynchronized receptors, plotted for fast dynamics in the $k_+c < k_-$ regime (CM in blue and BM in red). Letters refer to panel labels (A-D). Dotted red line indicates uncertainty from FM for comparison. (Inset) Same for a system of two receptors only.

Supporting Informations: *Accurate encoding and decoding by single cells: amplitude versus frequency modulation*

Gabriele Micali,^{1,2,3} Gerardo Aquino,^{1,2} David M. Richards,^{1,2} and Robert G. Endres^{1,2,*}

¹*Department of Life Sciences, Imperial College, London, UK*

²*Centre for Integrative System Biology and Bioinformatics, Imperial College, London, UK*

³*Dipartimento di Fisica, Università degli Studi di Milano, Milano, Italy*

TEXT S1

CONCENTRATION SENSING BY CM RECEPTOR

In this section we calculate the analytic solution for the master equation (Eq. ??,b in the main text) for continuous modulation (CM). For clarity, we repeat here the master equations for the *on* and *off* states:

$$\begin{aligned}\frac{dp_{\text{on}}(n,t)}{dt} &= \gamma(n+1)p_{\text{on}}(n+1,t) + \alpha p_{\text{on}}(n-1,t) + k_{+c} p_{\text{off}}(n,t) - (\gamma n + \alpha + k_{-})p_{\text{on}}(n,t), \\ \frac{dp_{\text{off}}(n,t)}{dt} &= \gamma(n+1)p_{\text{off}}(n+1,t) + k_{-} p_{\text{on}}(n,t) - (\gamma n + k_{+c})p_{\text{off}}(n,t),\end{aligned}$$

where $p_{\text{on/off}}(n,t)$ is the probability that the receptor/ion channel is in the *on/off* state with n output proteins at time t , α and γ are the production and degradation rates respectively, and k_{+c} and k_{-} are the binding and unbinding rates respectively. Note that the concentration of the input species (c) is now constant. Eqs. (??,b) can be rewritten as Eq. (??) in the main text

$$\frac{dp_s(n,t)}{dt} = \gamma(n+1)p_s(n+1,t) + \alpha_s p_s(n-1,t) + k_{\bar{s}} p_{\bar{s}}(n,t) - (\gamma n + \alpha_s + k_s)p_s(n,t),$$

where \bar{s} is the *on/off* state when s is the *off/on* state, and $\alpha_{\text{on}} = \alpha$, $\alpha_{\text{off}} = 0$, $k_{\text{on}} = k_{-}$ and $k_{\text{off}} = k_{+c}$. To find the solution for the first two moments of the distribution $p(n,t)$, we now follow Mehta and Schwab [1]. At steady state Eq. (??) becomes

$$K_{\bar{s}} p_{\bar{s}}(n) = -(n+1)p_s(n+1) - A_s p_s(n-1) + (n + A_s + K_s)p_s(n), \quad (\text{S2})$$

where $K_s = k_s/\gamma$ and $A_s = \alpha_s/\gamma$. Using the generating function in Eq. (??)

$$G_s(z) = \sum_{n=0}^{\infty} p_s(n)z^n,$$

Eq. (S2) becomes

$$[(z-1)\partial_z - A_s(z-1) + K_s] G_s(z) = K_{\bar{s}}, \quad (\text{S3})$$

which implies

$$(\partial_z - A_{\text{on}}) G_{\text{on}} = \frac{K_{\text{off}} G_{\text{off}} - K_{\text{on}} G_{\text{on}}}{z-1}, \quad (\text{S4})$$

$$(\partial_z - A_{\text{off}}) G_{\text{off}} = \frac{K_{\text{on}} G_{\text{on}} - K_{\text{off}} G_{\text{off}}}{z-1}, \quad (\text{S5})$$

which, when combined, gives

$$(\partial_z - A_{\text{on}}) G_{\text{on}} = -(\partial_z - A_{\text{off}}) G_{\text{off}}. \quad (\text{S6})$$

* r.endres@imperial.ac.uk

To proceed further, it is useful to define the quantity $H_s(z)$ related to the generating function $G_s(z)$ by

$$G_s(z) = e^{A_s z} H_s(z). \quad (\text{S7})$$

Using

$$\left(\partial_z - A_s\right) G_s(z) = e^{A_s z} \partial_z H_s(z), \quad (\text{S8})$$

Eq. (S6) becomes

$$e^{A_{\text{on}} z} \partial_z H_{\text{on}}(z) = -e^{A_{\text{off}} z} \partial_z H_{\text{off}}(z), \quad (\text{S9})$$

which links the expressions for H_{on} and H_{off} . At this point the initial equation for the steady state (Eq. (S3)) becomes

$$(z-1)e^{A_s z} \partial_z H_s(z) + K_s e^{A_s z} \partial_z H_s(z) = K_{\bar{s}} e^{A_{\bar{s}} z} \partial_z H_{\bar{s}}(z). \quad (\text{S10})$$

Multiplying by $e^{A_{\bar{s}} z}$, taking the derivative with respect to z , substituting Eq. (S9), and defining $\Delta A_s = A_{\bar{s}} - A_s$, gives

$$\partial_z H_s(z) - \Delta A_s (z-1) \partial_z H_s(z) + (z-1) \partial_z^2 H_s(z) - K_s \Delta A_s H_s(z) + K_s \partial_z H_s(z) = -K_{\bar{s}} H_s(z)$$

and hence

$$(z-1) \partial_z^2 H_s(z) + \left(1 - \Delta A_s (z-1) + K_s + K_{\bar{s}}\right) \partial_z H_s(z) - K_s \Delta A_s H_s(z) = 0.$$

Finally, changing variables to $u = \Delta A_s (z-1)$ provides

$$u \partial_z^2 H_s(u) + (1 + K_s + K_{\bar{s}} - u) \partial_z H_s(u) - K_s H_s(u) = 0. \quad (\text{S11})$$

This is the confluent hypergeometric equation, for which the solution in terms of confluent hypergeometric functions of the first kind is given by

$$H_s(u) = c_s {}_1F_1(K_s, 1 + K_s + K_{\bar{s}}; u), \quad (\text{S12})$$

with c_s a constant of integration. Thus, through Eq. (S7),

$$G_s(z) = c_s e^{A_s z} {}_1F_1(K_s, 1 + K_s + K_{\bar{s}}; \Delta A_s (z-1)). \quad (\text{S13})$$

To determine the constants, notice that ${}_1F_1(a, b, 0) = 1$ leading to

$$G_s(1) = c_s e^{A_s} = \langle p_s \rangle = \frac{K_{\bar{s}}}{K_{\bar{s}} + K_s},$$

where $\langle p_s \rangle$ is the average probability of being in state s . Rearranging terms, we obtain

$$c_s = \frac{K_{\bar{s}}}{K_{\bar{s}} + K_s} e^{-A_s}. \quad (\text{S14})$$

Finally, the probability distribution at steady state is given by [1]

$$G_s(z) = \frac{K_{\bar{s}} e^{A_s (z-1)}}{K_{\bar{s}} + K_s} {}_1F_1(K_s, 1 + K_s + K_{\bar{s}}; \Delta K_2^s (z-1)). \quad (\text{S15})$$

Having an analytic expression for the steady-state probability distribution (Eq. S15), we can now calculate the first, second and third moments, which are related to the mean, variance and skewness, respectively. The mean production of the output protein is given by the mean production in the *on* state multiplied by the probability to be in the *on* state, averaged over the whole time period. For such a two-state system $\langle p_{\text{on}} \rangle = \frac{K_{\text{off}}}{K_{\text{off}} + K_{\text{on}}}$ and $\langle p_{\text{off}} \rangle = 1 - \langle p_{\text{on}} \rangle$. Therefore, the mean number of proteins is given by

$$\langle n \rangle = (A_{\text{on}} - A_{\text{off}}) \langle p_{\text{on}} \rangle + A_{\text{off}} = \frac{\alpha}{\gamma} \frac{k_+ c / k_-}{1 + k_+ c / k_-}. \quad (\text{S16})$$

To calculate the variance, we use the following property of the generating function:

$$(\delta n)^2 = \sum_s (\partial_z z \partial_z G_s(z)) \Big|_{z=1} - \langle n \rangle^2. \quad (\text{S17})$$

Proof.

$$\begin{aligned}
(\delta n)^2 &= \sum_s \left[\sum_n n^2 p_s(n) \right] - \langle n \rangle \\
&= \sum_s \left[\sum_n n^2 p_s(n) \right]_{z=1} - \langle n \rangle \\
&= \sum_s \left[\sum_n z \partial_z (n p_s(n) z^n) n^2 p_s(n) \right]_{z=1} - \langle n \rangle \\
&= \sum_s [z \partial_z z \partial_z G_s(z)]_{z=1} - \langle n \rangle \\
&= \sum_s [\partial_z z \partial_z G_s(z)]_{z=1} - \langle n \rangle.
\end{aligned}$$

□

Using common properties of hypergeometric functions, the analytical solution for the variance is [1]

$$\langle (\delta n)^2 \rangle = \langle n \rangle + \langle p_{\text{on}} \rangle \langle p_{\text{off}} \rangle \frac{(\Delta A_s)^2}{1 + K_s + K_{\bar{s}}} = \langle n \rangle + \frac{\alpha^2}{\gamma(\gamma + k_- + k_+ c)} \frac{k_+ c / k_-}{(1 + k_+ c / k_-)^2}. \quad (\text{S18})$$

For details, see the full calculation in the SI of [1].

Third moment

In order to understand more about the symmetry of the probability distribution, we calculate the third moment at steady state. As in Eq. (S17) the third moment can be found via generating functions as

$$\langle n^3 \rangle = \sum_s [\partial_z z \partial_z z \partial_z G_s(z)] \Big|_{z=1} = \sum_s [3z \partial_z^2 G_s(z) + z^2 \partial_z^3 G_s(z) + \partial_z G_s(z)] \Big|_{z=1}, \quad (\text{S19})$$

where [1]

$$\begin{aligned}
\sum_s \partial_z G_s(z) \Big|_{z=1} &= \langle n \rangle, \quad (\text{S20}) \\
\sum_s (z \partial_z^2 G_s(z)) \Big|_{z=1} &= \langle p_{\text{on}} \rangle (A_{\text{on}})^2 + \langle p_{\text{off}} \rangle (A_{\text{off}})^2 - \langle p_{\text{on}} \rangle \langle p_{\text{off}} \rangle \frac{\Delta A_s (K_{\text{on}} + K_{\text{off}})}{1 + K_s + K_{\bar{s}}} \\
&= \frac{\alpha^2 (k_+ c / k_-)}{\gamma^2 (1 + k_+ c / k_-)} + \frac{\alpha (k_+ c)}{\gamma (1 + k_+ c / k_-) (\gamma + k_- + k_+ c)}. \quad (\text{S21})
\end{aligned}$$

Thus, only $\sum_s z^2 \partial_z^3 G_s(z) \Big|_{z=1}$ needs to be calculated. The result is

$$\begin{aligned}
\sum_s (z^2 \partial_z^3 G_s(z)) \Big|_{z=1} &= (A_{\text{on}})^3 \langle p_{\text{on}} \rangle + (A_{\text{off}})^3 \langle p_{\text{off}} \rangle - \frac{\langle p_{\text{on}} \rangle \langle p_{\text{off}} \rangle (\Delta A_{\text{on}})^2 (K_{\text{on}} + K_{\text{off}})}{1 + K_{\text{on}} + K_{\text{off}}} \\
&\quad \times \left[\frac{(3 + K_{\text{on}} + 2K_{\text{off}}) A_{\text{on}}}{2 + K_{\text{on}} + K_{\text{off}}} + \frac{(3 + 2K_{\text{on}} + K_{\text{off}}) A_{\text{off}}}{2 + K_{\text{on}} + K_{\text{off}}} \right] \\
&= \frac{\alpha^3 (k_+ c / k_-)}{\gamma^3 (1 + k_+ c / k_-)} - \frac{\alpha^3 (k_+ c / k_-) (3\gamma + k_- + 2k_+ c)}{\gamma^3 (1 + k_+ c / k_-) (\gamma + k_- + k_+ c) (2\gamma + k_- + k_+ c)}. \quad (\text{S22})
\end{aligned}$$

By combining Eqs. (S57)-(S59) as indicated in Eq. (S56), we obtain the analytic expression for the skewness of our system.

Proof. From the definition of confluent hypergeometric functions of the first kind

$${}_1F_1(a, b; z) = \sum_{n=0}^{\infty} \frac{a_n}{b_n n!} z^n,$$

with

$$\begin{aligned} a_n &= a(a+1)(a+2)\dots(a+n-1), \\ b_n &= b(b+1)(b+2)\dots(b+n-1), \end{aligned}$$

and the fact that

$$z \partial_z {}_1F_1(a, b; z) = z \frac{a}{b} {}_1F_1(a+1, b+1; z), \quad (\text{S23})$$

we obtain

$$\partial_z G_s(z) = \frac{K_{\bar{s}}}{K_{\bar{s}} + K_s} \left[A_s e^{A_s(z-1)} {}_1F_1(\cdot, \cdot, \Delta A_s(z-1)) + \frac{\Delta A_s K_s}{1 + K_s + K_{\bar{s}}} e^{A_s(z-1)} {}_1F_1(+, +, \Delta A_s(z-1)) \right], \quad (\text{S24})$$

where $\Delta A_s = A_{\bar{s}} - A_s$ and ${}_1F_1(+, +, z) = {}_1F_1(a+1, b+1, z)$. We now need to calculate $\sum_s z^2 \partial_z^3 G_s(z) \Big|_{z=1}$. Using Eq. (S21) we find that

$$\begin{aligned} (z^2 \partial_z^3 G_s(z)) \Big|_{z=1} &= \frac{z^2 K_{\bar{s}}}{K_{\bar{s}} + K_s} \partial_z \left[\left((A_s)^2 {}_1F_1(\cdot, \cdot, \Delta A_s(z-1)) + \frac{2 \Delta A_s K_s A_s}{1 + K_s + K_{\bar{s}}} {}_1F_1(+, +, \Delta A_s(z-1)) \right. \right. \\ &\quad \left. \left. + \frac{(\Delta A_s)^2 K_s (K_s + 1)}{(1 + K_s + K_{\bar{s}})(2 + K_s + K_{\bar{s}})} \cdot {}_1F_1(+, +, +, \Delta A_s(z-1)) \right) e^{A_s(z-1)} \right] \Big|_{z=1}. \quad (\text{S25}) \end{aligned}$$

Differentiating and using property (S23), we obtain

$$\begin{aligned} (z^2 \partial_z^3 G_s(z)) \Big|_{z=1} &= \frac{z^2 K_{\bar{s}}}{K_{\bar{s}} + K_s} e^{A_s(z-1)} \left[(A_s)^3 {}_1F_1(\cdot, \cdot, \Delta A_s(z-1)) \right. \\ &\quad + \frac{3 \Delta A_s K_s (A_s)^2}{1 + K_s + K_{\bar{s}}} {}_1F_1(+, +, \Delta A_s(z-1)) \\ &\quad + \frac{3 (\Delta A_s)^2 K_s (K_s + 1) K_s}{(1 + K_s + K_{\bar{s}})(2 + K_s + K_{\bar{s}})} {}_1F_1(+, +, +, \Delta A_s(z-1)) \\ &\quad \left. + \frac{(\Delta A_s)^3 K_s (K_s + 1) (K_s + 2)}{(1 + K_s + K_{\bar{s}})(2 + K_s + K_{\bar{s}})(3 + K_s + K_{\bar{s}})} {}_1F_1(+, +, +, +, \Delta A_s(z-1)) \right] \Big|_{z=1}. \quad (\text{S26}) \end{aligned}$$

Evaluating at $z = 1$, we obtain

$$(z^2 \partial_z^3 G_s(z)) \Big|_{z=1} = \frac{K_{\bar{s}}}{K_{\bar{s}} + K_s} \left[(A_s)^3 + \frac{\Delta A_s K_s}{1 + K_s + K_{\bar{s}}} \left(3(A_s)^2 + \frac{\Delta A_s (K_s + 1)}{2 + K_s + K_{\bar{s}}} \left(3A_s + \frac{\Delta A_s (K_s + 2)}{3 + K_s + K_{\bar{s}}} \right) \right) \right]. \quad (\text{S27})$$

Finally, summing on the possible states of s we arrive at Eq. (S22). \square

SMALL-NOISE APPROXIMATION TO RAMP SENSING

Input noise

In the Model section of the main text, we built a model for a single receptor/ion channel that encodes information from an cell-external environment in some cell-internal degrees of freedom. Similarly to [2], we assume that the receptor/ion channel activity ($r(t)$) is a two state system: *on* with $r = 1$ when the receptor is bound or the channel open, and *off* with $r = 0$ when the receptor is not bound or the channel is closed. The external concentration ($c(t)$) is assumed to affect the unbound/closed time interval $\langle \tau_u \rangle = [k_+ c(t)]^{-1}$ but not the bound/open time interval $\langle \tau_b \rangle = k_-^{-1}$, where k_+ and k_- are both constants. Both interval durations are assumed to be independent, exponentially distributed random variables. The independence of binding and unbinding (or equivalently of opening and closing)

means that the probability of a molecule binding the receptor a second time is negligible. We therefore assume the system to be in the fast diffusion regime.

The signaling rate, called u , implements two different mechanisms of encoding, either continuous (CM) or bursty (BM) modulation. CM and BM ultimately correspond to amplitude (AM) and frequency (FM) modulation, respectively, when generalized to multiple receptors/ion channels as explained in the Results section of the main text. In CM the proteins are produced with a constant rate α during the binding time. On the other hand, for BM a burst of ζ proteins is realized at the time of binding, so

$$u(t) = \begin{cases} \alpha r(t) & \text{for CM} \\ \zeta \sum \delta(t - t_i^+) & \text{for BM,} \end{cases} \quad (\text{S28})$$

where $\alpha k_-^{-1} = \zeta$ and t_i^+ the binding times. By taking the average of the rate $u(t)$ over a time \tilde{t} much longer than both the average bound time, $\langle \tau_b \rangle = k_-^{-1}$, and the average unbound time, $\langle \tau_u \rangle = [k_+ c(t)]^{-1}$, but shorter than the time during which the external concentration changes, we obtain

$$\langle u(t) \rangle = \zeta \frac{k_+ c(t)}{1 + k_+ c(t)/k_-}, \quad (\text{S29})$$

$$\langle \delta u(t) \rangle = 0,$$

$$\langle \delta u(t) \delta u(t') \rangle = g \zeta^2 \frac{k_+ c(t)}{(1 + k_+ c(t)/k_-)^3} \delta(t - t'), \quad (\text{S30})$$

$$g = \begin{cases} 2 & \text{for CM} \\ 1 + [k_+ c(t)/k_-]^2 & \text{for BM,} \end{cases} \quad (\text{S31})$$

which become Eqs. (??), (??) and (??) in the main text by setting $\zeta = 1$. (See Supplementary Information in [2] for further details). Importantly, $g_{\text{BM}} < g_{\text{CM}}$ since $k_+ c(t) < k_-$, *i.e.* $\langle \tau_b \rangle < \langle \tau_u \rangle$.

By considering an external concentration given by Eq. (??) in the main text,

$$c(t) = \begin{cases} c_0 + c_1 t, & t \geq 0 \\ c_0, & t < 0, \end{cases}$$

with $c_1 t \ll c_0$, Eq. (S29) becomes

$$u(t) = \zeta \begin{cases} u_0 + u_1 t + \delta u(t), & t \geq 0 \\ u_0 + \delta u(t), & t < 0, \end{cases} \quad (\text{S32})$$

where we assume $\delta u(t) \ll u_0 + u_1 t$ and

$$u_0 = \frac{k_+ c_0}{(1 + k_+ c_0/k_-)}, \quad (\text{S33})$$

$$u_1 = \frac{k_+ c_1}{(1 + k_+ c_0/k_-)^2}, \quad (\text{S34})$$

$$\langle \delta u(t) \delta u(t') \rangle_{t, t' \geq 0} = \begin{cases} \frac{\delta(t-t')}{(1+k_+c_0/k_-)^2} [g_{\text{CM}} u_0 + g_{\text{CM}} (1 - 2k_+c_0/k_-) u_1 t] & \text{for CM} \\ \frac{\delta(t-t')}{(1+k_+c_0/k_-)^2} [g_{\text{BM}}^* u_0 + (1 - 2k_+c_0/k_- + 3k_+^2 c_0^2/k_-^2) u_1 t] & \text{for BM,} \end{cases} \quad (\text{S35})$$

$$\langle \delta u(t) \delta u(t') \rangle_{t, t' < 0} = \frac{g u_0}{(1 + k_+ c_0/k_-)^2} \delta(t - t'). \quad (\text{S36})$$

Here $g_{\text{CM}} = 2$ and $g_{\text{BM}}^* = 1 + (k_+ c_0/k_-)^2$ (cf. Eq. (??) in the main text). Again for $\zeta = 1$, this becomes Eq. (??) in the main text. From Eqs. (S32)-(S36), the constant ($t < 0$) and ramp ($t \geq 0$) regimes for the external species c are encoded in the rate u in the corresponding regimes since the condition $c_1 t \ll c_0$ ensures $u_1 t \ll u_0$. However, to satisfy condition $\delta u \ll \langle u \rangle$ for both CM and BM, a new condition is needed:

$$\frac{g_{\text{CM/BM}}}{k_+ c_0 (1 + k_+ c_0/k_-)} \ll \tau_c, \quad (\text{S37})$$

which implies

$$k_-, k_+ c_0 \gg \tau_c^{-1}. \quad (\text{S38})$$

Here, we have introduced the correlation time of white noise, τ_c , corresponding to the δ -function used in Eqs.(S35) and (S36). Note that condition in (S38) restricts our study to the fast switching regime. Finally, the signaling rate u in the constant regime has one small term $\delta u/u_0$ of order δ which is defined by Eqs. (S32) and (S36). Instead, small-ramp regime u contains two small terms: the small-ramp term $u_1 t/u_0$ of order ϵ and the small noise term $\delta u/u_0$ which now has a correction to order δ coming from the small ramp (order ϵ). With these definitions, from Eqs. (S32)-(S35) the rate u in the small ramp regime has two small corrections to the constant rate u_0

$$u(t) = \zeta u_0 \left(1 + \underbrace{\frac{u_1 t}{u_0}}_{o(\epsilon)} + \underbrace{\frac{\delta u}{u_0}}_{o(\delta(1+\sqrt{\epsilon}))} \right), \quad (\text{S39})$$

In order to linearize around linear solutions, we further assume that the small-noise amplitude is smaller than the small ramp. As a result, $o(\delta) \sim o(\epsilon^x)$ with $x > 1$, which means that

$$g(1 + k_+ c_0/k_-) k_+ c_0 < \tau_c (k_+ c_1 t)^2. \quad (\text{S40})$$

Note that for simplicity, both in the following sections and in the main text, we set $\zeta = 1$.

Output noise in incoherent feedforward loop

Average solutions for ramp sensing

Eqs. (??) and (??) in the main text for the incoherent feedforward loop for $f(u) = e^{bu}$ and $g(y) = e^{-bk_y y}$ become

$$\frac{dx}{dt} = k_x \left[e^{b(u-k_y y)} - x \right], \quad (\text{S41})$$

$$\frac{dy}{dt} = u - k_y y. \quad (\text{S42})$$

Here, b is a constant introduced to maintain the exponent unitless, and k_x and k_y are rate constants for x and y . This system of equations performs exact adaptation. The steady-state solution in the constant regime ($t < 0$ in Eq. (S32)) is

$$\langle x(t) \rangle = 1, \quad \langle y(t) \rangle = \frac{u_0}{k_y}, \quad (\text{S43})$$

which sets the initial conditions $\langle x(0) \rangle = 1$ and $\langle y(0) \rangle = u_0/k_y$ for Eqs. (S41) and (S42) in the ramp regime ($t \geq 0$ in Eq. ??). With these initial conditions, the solutions for $t \geq 0$ can be written as

$$\langle x(t) \rangle = e^{-k_x t} k_x e^{\frac{bu_1}{k_y}} \int_0^t dt' e^{k_x t' - \frac{bu_1}{k_y}} e^{-k_y t'}, \quad (\text{S44})$$

$$\langle y(t) \rangle = \frac{u_0}{k_y} - \frac{u_1}{k_y^2} + \frac{u_1}{k_y} t + \frac{u_1}{k_y^2} e^{-k_y t}, \quad (\text{S45})$$

where the integral in the expression for $\langle x(t) \rangle$ cannot be solved analytically. However, by assuming that the integral starts from time $\epsilon \gg k_y^{-1}$, Eq. (S44) becomes

$$\langle x(t) \rangle \simeq e^{\frac{bu_1}{k_y}} + e^{-k_x(t-\epsilon)} \left[\langle x(\epsilon) \rangle - e^{\frac{bu_1}{k_y}} \right].$$

Finally, by considering t such that $t - \epsilon \gg k_x^{-1}$ and without exceeding the small-ramp regime (e.g. $k_{x,y} \gg 1$ and ϵ small), the solution becomes Eqs. (??-b) in the main text,

$$\begin{aligned} \langle x(t) \rangle &= e^{\frac{bu_1}{k_y}}, \\ \langle y(t) \rangle &= \frac{u_0}{k_y} - \frac{u_1}{k_y^2} + \frac{u_1}{k_y} t. \end{aligned}$$

These solutions match numerical results shown in S4A Fig. Note that the time interval over which these solutions are valid extends from a time larger than the transient time to around a time that does not exceed the small-ramp regime. These criteria also set the regime of validity for our next results.

Output variances in ramp sensing

Above we gave the average solutions for the incoherent feedforward loop, both in the constant regime ($t < 0$, Eq. (S43)) and in the ramp regime ($t \geq 0$, Eqs. (S44) and (S45)). Now we want to linearize the equations around these solutions in order to obtain information about the noise. We assume that the input noise (δu) is smaller than the ramp, Eqs. (S38) and (S40), which translates into small output noise (δx and δy). In addition to these assumptions, we also assume $b \sim u_0^{-1}$ in order to ensure $b(\delta u - k_y \delta y) \ll 1$. Hence, in the ramp regime, the differential equations for δx and δy become

$$\frac{d(\delta x)}{dt} = k_x \left[b e^{\frac{u_+ b}{k_y}} (\delta u - k_y \delta y) - \delta x \right], \quad (\text{S47})$$

$$\frac{d(\delta y)}{dt} = \delta u - k_y \delta y. \quad (\text{S48})$$

By defining $X(t) = \begin{bmatrix} \delta x \\ \delta y \end{bmatrix}$, Eqs. (S47) and (S48) can be rewritten in a compact way for both the constant and small-ramp regimes as

$$\frac{dX(t)}{dt} + M(t)X(t) = \begin{bmatrix} A(t)\delta u(t) \\ \delta u(t) \end{bmatrix}, \quad (\text{S49})$$

where

$$M(t) = \begin{cases} \begin{bmatrix} k_x & k_x k_y b \\ 0 & k_y \end{bmatrix}, & t < 0 \\ \begin{bmatrix} k_x & k_x k_y b e^{\frac{b u_+}{k_y}} \\ 0 & k_y \end{bmatrix}, & t \geq 0, \end{cases} \quad (\text{S50})$$

and

$$A(t) = \begin{cases} k_x b, & t < 0 \\ k_x b e^{\frac{b u_+}{k_y}}, & t \geq 0. \end{cases} \quad (\text{S51})$$

Note that $M(t)$ (for $t > 0$) is independent of time, which allows Eq. (S49) to be solved analytically. This is due to our choice of $f(u)$ and $g(u)$ in Eqs. (??) and (??) in the main text.

For the constant input regime, $t < 0$, the solutions for CM and BM are

$$\langle (\delta x(t))^2 \rangle = \frac{g_{\text{CM/BM}} b^2 k_x^2 u_0}{2(k_x + k_y)(1 + k_+ c_0 / k_-)^2}, \quad (\text{S52})$$

$$\langle (\delta y(t))^2 \rangle = \frac{g_{\text{CM/BM}} u_0}{2k_y(1 + k_+ c_0 / k_-)^2}, \quad (\text{S53})$$

where $g_{\text{CM}} = 2$ and $g_{\text{BM}} = g_{\text{BM}}^* = 1 + (k_+ c_0 / k_-)^2$. Hence, in the constant regime the output noise for BM is lower than the output noise for CM since $k_+ c_0 < k_-$.

For the small-ramp regime, $t \geq 0$, Eq. (S49) is analytically solvable for $t \gg k_y^{-1}$ by evaluating the integral from time $\epsilon \gg k_y^{-1}$ to some time t that does not exceed the small-ramp approximation (as discussed for the average solutions). With these assumptions and by using an appropriate integrating factor, the solution for $X(t)$ is

$$\int_{\epsilon}^t e^{Mt'} \frac{dX(t')}{dt'} dt' + \int_{\epsilon}^t e^{Mt'} M X(t') dt' = \int_{\epsilon}^t e^{Mt'} \begin{bmatrix} A \delta u(t') \\ \delta u(t') \end{bmatrix} dt',$$

$$X(t) = e^{-Mt} \int_{\epsilon}^t e^{Mt'} \begin{bmatrix} A \delta u(t') \\ \delta u(t') \end{bmatrix} dt' + e^{-M(t-\epsilon)} X(\epsilon).$$

However, for $t - \epsilon \gg k_{x,y}^{-1}$ (within the limit for t and ϵ as discussed for Eqs. (??,b) the solution is

$$X(t) = e^{-Mt} \int_{\epsilon}^t e^{Mt'} \begin{bmatrix} A \delta u(t') \\ \delta u(t') \end{bmatrix} dt'. \quad (\text{S54})$$

By using matrix diagonalization, expressing the noise in u by a delta function in time (Eq. S35), and integrating Eq. (S54) for $X(t)^2$, we find analytical solutions for the variances. The results for CM are

$$\langle (\delta x(t))^2 \rangle_{\text{CM}} = \frac{b^2 k_x^2 e^{\frac{2bu_1}{k_y}}}{2(k_x + k_y)(1 + k_+ c_0/k_-)^2} \left[g_{\text{CM}} u_0 - g_{\text{CM}} \frac{(1 - 2k_+ c_0/k_-)}{k_x + k_y} u_1 + g_{\text{CM}} (1 - 2k_+ c_0/k_-) u_1 t \right], \quad (\text{S55})$$

$$\langle (\delta y(t))^2 \rangle_{\text{CM}} = \frac{1}{2k_y(1 + k_+ c_0/k_-)^2} \left[g_{\text{CM}} u_0 - g_{\text{CM}} \frac{(1 - 2k_+ c_0/k_-)}{k_y} u_1 + g_{\text{CM}} (1 - 2k_+ c_0/k_-) u_1 t \right], \quad (\text{S56})$$

where $g_{\text{CM}} = 2$. For BM, the g_{BM} parameter (see Eq. (??)) affects the integration, and the results are

$$\langle (\delta x(t))^2 \rangle_{\text{BM}} = \frac{b^2 k_x^2 e^{\frac{2bu_1}{k_y}}}{2(k_x + k_y)(1 + k_+ c_0/k_-)^2} \left[g_{\text{BM}}^* u_0 - \frac{1 - 2k_+ c_0/k_- + 3k_+^2 c_0^2/k_-^2}{k_x + k_y} u_1 + (1 - 2k_+ c_0/k_- + 3k_+^2 c_0^2/k_-^2) u_1 t \right], \quad (\text{S57})$$

$$\langle (\delta y(t))^2 \rangle_{\text{BM}} = \frac{1}{2k_y(1 + k_+ c_0/k_-)^2} \left[g_{\text{BM}}^* u_0 - \frac{1 - 2k_+ c_0/k_- + 3k_+^2 c_0^2/k_-^2}{2k_y} u_1 + (1 - 2k_+ c_0/k_- + 3k_+^2 c_0^2/k_-^2) u_1 t \right], \quad (\text{S58})$$

where $g_{\text{BM}}^* = 1 + (k_+ c_0/k_-)^2$. Note that for $c_1 = u_1 = 0$, the solutions coincide with the solutions for the constant regime. Furthermore, by comparing the time-dependent terms, CM is noisier than BM when $k_+ c_0 < \frac{1}{3} k_-$. In our model this is due to the input noise (cf. Eq. S35). These two regimes in which BM is less noisy and hence more accurate than CM depend on the ratio of binding and unbinding rates as shown in S4B,C Fig. Clearly the analytic solutions match numerical simulations with noise. All these calculations were done using Wolfram Mathematica 8, while all the simulations of the stochastic differential equations (Eqs. S41 and S42) were done using the Euler method in MATLAB.

Output noise for integral feedback loop

A similar approach can be applied to the integral feedback loop given by Eqs. (??) and (??) in the main text, shown here for clarity with $f(y) = e^{-by}$:

$$\frac{dx}{dt} = ue^{-by} - k_x x, \quad (\text{S59})$$

$$\frac{dy}{dt} = k_y (x - 1). \quad (\text{S60})$$

Assuming that u is given by Eq. (S32), this system does not have analytic solutions in the ramp regime. However, in the small-ramp regime it is possible to linearize around the solutions of the constant regime. Hence, $\langle x(t) \rangle = x_0 + \epsilon_x(t)$ and $\langle y(t) \rangle = y_0 + \epsilon_y(t)$, where $x_0 = 1$ and $y_0 = \frac{\ln(u_0/k_x)}{b}$ are the solutions for the constant regime with $\langle u \rangle = u_0$. Note that the condition $k_x < u_0$ is required. By linearization, Eqs. (??) and (??) become

$$\frac{d\epsilon_x(t)}{dt} = k_x \frac{u_1 t}{u_0} - k_x \epsilon_x(t) - k_x b \epsilon_y(t) - b k_x \frac{u_1}{u_0} \epsilon_y(t) t, \quad (\text{S61})$$

$$\frac{d\epsilon_y(t)}{dt} = k_y \epsilon_x(t). \quad (\text{S62})$$

Combining both equations and neglecting the second-order term $u_1 t/u_0 \epsilon_y(t)$, it possible to find a second-order differential equation for $\epsilon_x(t)$, given by

$$\frac{d^2 \epsilon_x(t)}{dt^2} + k_x \frac{d\epsilon_x(t)}{dt} + b k_x k_y \epsilon_x(t) = \frac{k_x u_1}{u_0}. \quad (\text{S63})$$

The solution is

$$\epsilon_x(t) = \frac{u_1}{b k_y u_0} + C_1 \exp \left[\left(-\frac{k_x}{2} - \sqrt{\frac{k_x^2}{4} - b k_x k_y} \right) t \right] + C_2 \exp \left[\left(-\frac{k_x}{2} + \sqrt{\frac{k_x^2}{4} - b k_x k_y} \right) t \right], \quad (\text{S64})$$

with $\epsilon_x(t) \rightarrow \frac{u_1}{bk_y u_0}$ after a transient time defined by the exponential terms for any $k_x^2/4 - bk_x k_y$. Furthermore, there are two integration constants C_1 and C_2 . From Eq. (S62) we obtain $\epsilon_y = \frac{u_1}{bu_0}t - \frac{u_1}{b^2 k_y u_0}$. Finally, the solutions of linearized Eqs. (??) and (??) in the small-ramp regime after the transient time are [2]

$$\langle x(t) \rangle = 1 + \frac{u_1}{bk_y u_0}, \quad (\text{S65})$$

$$\langle y(t) \rangle = y_0 - \frac{u_1}{b^2 k_y u_0} + \frac{u_1}{bu_0}t. \quad (\text{S66})$$

Within the small-noise approximation (Eq. S38), we want to find expressions for the variances. In the constant regime, $u(t) = u_0 + \delta u(t)$ ($t < 0$ in Eq. 5) implies $x(t) = 1 + \delta x(t)$ and $y(t) = y_0 + \delta y(t)$. Therefore, the equations for the noise terms become

$$\frac{d(\delta x)}{dt} = k_x \left[\frac{\delta u}{u_0} - bu_0 \delta y - \delta x \right], \quad (\text{S67})$$

$$\frac{d(\delta y)}{dt} = k_x \delta x. \quad (\text{S68})$$

Proceeding similarly to the incoherent feedforward loop, in the constant regime the solution for the variances are [2]

$$\langle (\delta x)^2 \rangle = \frac{g_{\text{CM/BM}} k_x}{2(1 + k_+ c_0 / k_-)^2 u_0}, \quad (\text{S69})$$

$$\langle (\delta y)^2 \rangle = \frac{g_{\text{CM/BM}} k_y}{2b(1 + k_+ c_0 / k_-)^2 u_0}, \quad (\text{S70})$$

with $g_{\text{CM}} = 2$ and $g_{\text{BM}} = g_{\text{BM}}^* = 1 + (k_+ c_0 / k_-)^2$. Hence, in the constant regime, the output noise for BM is lower than the output noise for CM (since $k_+ c_0 < k_-$).

To study the system in the small-ramp regime ($t > 0$ in Eq. 5), we assume that the input noise (δu) is smaller than the ramp (Eqs. S38 and S40), which translates into small output noise (δx and δy), and linearize around solutions (S65) and (S66). As a result, Eq. (??) becomes

$$\frac{d(\delta x)}{dt} = k_x \left[\left(1 + \frac{u_1 t}{u_0} + \frac{\delta u}{u_0} \right) \left(1 - b(\epsilon_y + \delta y) + \frac{b^2}{2}(\epsilon_y + \delta y)^2 \right) - 1 - \epsilon_x - \delta x \right],$$

which, by using Eq. (S61), becomes

$$\frac{d(\delta x)}{dt} = k_x b \left[\frac{\delta u}{u_0} - \delta y - \frac{u_1}{u_0} \epsilon_y t - \frac{u_1 t}{u_0} \delta y - \frac{\epsilon_y}{u_0} \delta u + \frac{b \epsilon_y^2}{2} + b \epsilon_y \delta y - \frac{\delta x}{b} + o(\epsilon^3, \delta^2, \epsilon^2 \delta) \right], \quad (\text{S71})$$

where we neglect third-order terms in the small ramp ($o(\epsilon^3)$), second-order terms in the small noise (δ^2) and mixed-order terms ($o(\epsilon^2 \delta)$) due to the assumption that the noise is smaller than the ramp (cf. discussion that leads to Eq. (S40)).

Defining $X(t) = \begin{bmatrix} \delta x \\ \delta y \end{bmatrix}$, Eqs. (S71) and (S60) become

$$\frac{dX(t)}{dt} + M(t)X(t) = \begin{bmatrix} A(t)\delta u(t) + B(t) \\ 0 \end{bmatrix}, \quad (\text{S72})$$

where from Eqs. (S71) and (S60), using definitions of ϵ_x and ϵ_y , $M(t) = \begin{bmatrix} k_x & k_x b \left(1 + \frac{bu_1}{k_y u_0} \right) \\ -k_y & 0 \end{bmatrix}$, $A(t) = \frac{k_x}{u_0} \left(1 + \frac{u_1}{k_y b u_0} - \frac{u_1 t}{u_0} \right)$ and $B(t) = \frac{k_x u_1^2}{u_0^2} \left(\frac{t}{k_y} - t^2 \right)$. Using an integrating factor and integrating between ϵ and t gives

$$X(t) = e^{-M(t-\epsilon)} X(\epsilon) + e^{-Mt} \int_{\epsilon}^t dz e^{Mz} A(z) \begin{bmatrix} \delta u \\ 0 \end{bmatrix} + e^{-Mt} \int_{\epsilon}^t dz e^{Mz} B(z) \begin{bmatrix} 1 \\ 0 \end{bmatrix}, \quad (\text{S73})$$

where the term $e^{-M(t-\epsilon)}X(\epsilon)$ is negligible for $(t-\epsilon) \gg k_{x,y}^{-1}$. To calculate the variances we square Eq. (S73). Using Eqs. (S5)-(S9), the results for $\langle(\delta x(t))^2\rangle$ to first-order in the small-ramp parameters are

$$\langle(\delta x(t))^2\rangle_{CM} = \frac{kx}{2(1+k_+c_0/k_-)^2 u_0} \left[g_{CM} - g_{CM}(1+2k_+c_0/k_-) \frac{u_1 t}{u_0} + g_{CM} \frac{2k_x + bk_y(1+2k_+c_0/k_-) u_1}{bk_y k_x u_0} \right], \quad (S74)$$

$$\langle(\delta x(t))^2\rangle_{BM} = \frac{kx}{2(1+k_+c_0/k_-)^2 u_0} \left[g_{BM}^* - (1+2k_+c_0/k_- - k_+^2 c_0^2/k_-^2) \frac{u_1 t}{u_0} + \frac{(bk_y(1+2k_+c_0/k_- - k_+^2 c_0^2/k_-^2) + 2k_x g_{BM}^*) u_1}{bk_x k_y u_0} \right]. \quad (S75)$$

Similarly the results for $\langle(\delta y)^2\rangle$ are

$$\langle(\delta y(t))^2\rangle_{CM} = \frac{k_y}{2b(1+\langle\tau_b\rangle k_+c_0)^2 u_0} \left[g_{CM} - g_{CM}(1+2k_+c_0/k_-) \frac{u_1 t}{u_0} + g_{CM} \frac{(kx(3+2k_+c_0/k_-) + 2k_y b(1+2k_+c_0/k_-)) u_1}{2bk_x k_y u_0} \right], \quad (S76)$$

$$\langle(\delta y(t))^2\rangle_{BM} = \frac{k_y}{2b(1+\langle\tau_b\rangle k_+c_0)^2 u_0} \left[g_{BM}^* - \left(1 + 2\langle\tau_b\rangle k_+c_0 - \langle\tau_b\rangle^2 k_+^2 c_0^2\right) \frac{u_1 t}{u_0} + \frac{\left[2bk_y \left(1 + 2\langle\tau_b\rangle k_+c_0 - \langle\tau_b\rangle^2 k_+^2 c_0^2\right) + k_x \left(3 + 2\langle\tau_b\rangle k_+c_0 + \langle\tau_b\rangle^2 k_+^2 c_0^2\right)\right] u_1}{bk_y k_x u_0} \right], \quad (S77)$$

where $g_{BM}^* = 1 + (k_+c_0/k_-)^2$. Note that for $c_1 = u_1 = 0$, the solutions coincide with the solutions for the constant regime. Although it is clear that BM is less noisy than CM for $k_+c_0 < k_-$, by comparing the time-dependent terms we find that, in fact, BM is always less noisy than CM. The analytical solutions are plotted in S5 Fig. and match the numerical simulations with noise. Again, all these calculations were done using Wolfram Mathematica 8, while all the simulations of the stochastic differential equations (Eqs. S59 and S60) were done using the Euler method in MATLAB.

FURTHER INVESTIGATIONS INTO THE ACCURACY

In this section we provide further explanations for the accuracy of concentration sensing by a single receptor without comparing with the maximum-likelihood estimation [3]. In Fig. ?? we showed results from the master equation for the two regimes $k_+c_0 < k_-$ and $k_+c_0 > k_-$ for slow and fast switching of the receptor. Despite its burstiness, the BM receptor turned out more accurate than the CM receptor in the $k_+c_0 < k_-$ regime for fast switching.

Additional results from the master-equation model. To understand this result better we also implemented an intermediate-modulation (IM) receptor, which has features of both the CM and BM receptors. Like the CM receptor, the IM receptor signals while in the bound (*on*) state, but instead of a constant rate α of production it produces protein with a rate α' so that in each bound interval the same number of molecules are produced irrespective of the interval length, i.e. $\alpha'\tau_b = \zeta$, with ζ the constant burst size of BM. For this to work, the IM receptor would have to know at the time of binding when it will unbind again, in order to choose the correct rate of production. Since the rate of unbinding is a random variable this is generally not possible. Nevertheless, the IM receptor may help to further elucidate our observed trends in accuracy. In practice, we implemented this IM receptor by first simulating a time trace of bound and unbound time intervals with a Gillespie algorithm, allowing us to determine the rate of production as a function of time. Afterwards, the actual protein production and degradation were simulated.

In analogy to Fig. ?? the results for the IM receptor are shown in S1 Fig. (green lines), which also shows the results for the CM and BM receptors for comparison in blue and red, respectively. As expected, for slow switching the IM receptor has intermediate accuracy between CM and BM. CM is most accurate as continuous production during the bound intervals is balanced by degradation so the output protein level does not fluctuate excessively. BM is least accurate due to the increased burst size for slow switching. Since signaling by the IM receptor is only burst-like for the short bound intervals but not for the long bound intervals, it is somewhat more accurate than BM. Due to the

non-constant rate of production, IM also fluctuates more than CM. This intermediate accuracy is clearly demonstrated by the time traces in the left panels of S2 Fig.

In the $k_+c_0 < k_-$ regime for fast switching, the inset of S1C Fig. shows that BM is now most accurate and that IM has again intermediate accuracy. While BM steadily produces the same amount of protein at the times of binding, IM produces this amount only during short bound intervals as its rate of production is then high, while during long bound intervals its slow production is buffered by degradation, so its protein level fluctuates more strongly. CM is even worse than IM since, due to its constant rate of production during bound time intervals, it hardly produces any protein during short bound intervals, which leads to drastic drops in protein level, while it produces a lot during long bound intervals due to its constant rate of production.

In contrast, in the $k_+c_0 > k_-$ regime for fast switching, CM is generally most accurate due to its approximately constant rate of production throughout time, i.e. the receptor is almost always bound and active. IM is less accurate than CM because its rate of protein production is variable due to the variable length in bound intervals, despite the fact that the receptor is mostly bound. Interestingly, IM is even less accurate than BM under these conditions. Inspecting the examples of time trace in the bottom right panel of S2 Fig., the burst sizes of IM can exceed the burst sizes of BM for unusually short bound intervals since production is very high and stochastic, and only on average the same amount of protein is produced during bound intervals than during a burst in BM. During long bound intervals the rate of production is very low. Hence, compared to BM, degradation prevents a net increase in protein level during a bound interval, leading to further variability. A special case is when the burst size ζ is 1. As shown in the inset of Fig. ??D, BM can be more accurate than CM. This is because the burst size of BM is minimal and in the master equation the production with minimal rate α in CM is highly stochastic.

As we now discuss, to provide further intuition for the differences in accuracy between the $k_+c_0 < k_-$ and $k_+c_0 > k_-$ regimes, we also simulated the variance of the signaling output (and hence the accuracy-determining factor g) directly (see Eq. 5).

Signaling output from ODE model without protein production and degradation. Factor g in Eq. 5 (and Eq. S31) determines the variance of the signaling rate $u(t)$ without invoking any downstream protein production and degradation. For a given time interval Δt , we can hence simulate $u(t)$ directly. We assess the accuracy of CM, IM, and BM by plotting the histograms of the integrated signaling rate $u_I(\Delta t) := \int_0^{\Delta t} u(t)dt$ and by determining their variances (cf. derivation of g in [2]). As slow protein production and degradation strongly affect the accuracy of the final protein output for slow switching, this approach mainly helps understand the interesting fast switching case.

We initially assume signaling during bound intervals is deterministic, leading to a linear increase of u with slope α (α') during a bound time interval for CM (IM) and a step increase by ζ for BM. At each unbound time interval, IM and BM have the same level of signaling output as IM produces the same number of proteins deterministically during each bound interval (ζ). In contrast, the signaling output from CM is generally different since the rate of signaling is always the same for each bound interval but their durations vary. Resulting time traces and variances are shown in S3A and B Figs. left panels, respectively. Specifically, S3A Fig., left panels shows clearly that for $k_+c_0 < k_-$ BM and IM are most accurate with $u_I(t)$ increasing almost linearly in time. Since signaling is deterministic, BM and IM are essentially identical, and their variance may only differ due to small differences in signaling during the final bound interval (S3A Fig., bottom left panel). This last bound time interval may be interrupted in IM, but for long Δt this difference is negligible. In contrast, S3B Fig., left panels show clearly that for $k_+c_0 > k_-$ CM is most accurate, as $u_I(t)$ is now almost linear in time.

Signaling output from master-equation model without protein production and degradation. Allowing signaling to be stochastic does not change the results for the accuracy significantly. S3A Fig. right panels show that for $k_+c_0 < k_-$ BM is now most accurate and that IM has intermediate accuracy (between BM and CM) due to its variability in signaling in line with S1C Fig. Additionally, S3B Fig., right panels show that CM is still most accurate but also that IM is worse than BM in line with S1D Fig.

Taken together, these additional simulation results confirm our findings of the main text that BM is most accurate for $k_+c_0 < k_-$ and CM is generally most accurate for $k_+c_0 > k_-$.

AM IS MORE ACCURATE THAN FM FOR MULTIPLE RECEPTORS/ION CHANNELS

Here, we provide a more detailed discussion of the accuracy of encoding by multiple receptors, i.e. using AM and FM. To determine whether AM or FM is more accurate in encoding and decoding, we generalize to multiple receptors (or ion channels) (S6 Fig.). We assume that AM is obtained by unsynchronized CM receptors (S6A Fig.), while FM is obtained by synchronized receptors that individually operate with BM (S6D Fig.). Other types of synchronization are also possible with synchronized CM receptors shown in S6B Fig. and unsynchronized BM receptors shown in

S6C Fig. However, these receptors exhibit imperfect FM: resulting bursts have either variable duration (S6B Fig.) or variable amplitude (S6C Fig.) in contrast to the data (Fig. ??) [4, 5].

To estimate the accuracy, we first consider perfect synchronization and unsynchronization in either modulation scheme. For N unsynchronized (*us*) receptors, we can express the resulting average and variance of the encoded input by the single-receptor quantities, i.e. $\langle u(t) \rangle_N^{us} = N \langle u(t) \rangle_1$ and $\langle \delta u(t) \delta u(t') \rangle_N^{us} = N \langle \delta u(t) \delta u(t') \rangle_1$. As a result, the relative variance (variance divided by the average-squared) scales with N^{-1} . In contrast, for N synchronized (*s*) receptors, the average and variance of the encoded input can be written as $\langle u(t) \rangle_N^s = N \langle u(t) \rangle_1$ and $\langle \delta u(t) \delta u(t') \rangle_N^s = N^2 \langle \delta u(t) \delta u(t') \rangle_1$, respectively. Hence, the relative variance is now independent of N , so unsynchronized receptors have an N times smaller noise than synchronized receptors. Since N unsynchronized CM receptors lead to AM, we obtain for its relative variance

$$\frac{\langle \delta u(t) \delta u(t') \rangle_N^{AM}}{\left(\langle u(t) \rangle_N^{AM} \right)^2} = \frac{\langle \delta u(t) \delta u(t') \rangle_1^{CM}}{N \left(\langle u(t) \rangle_1^{CM} \right)^2}. \quad (S78)$$

Conversely since N synchronized BM receptors lead to FM, the relative variance of FM is

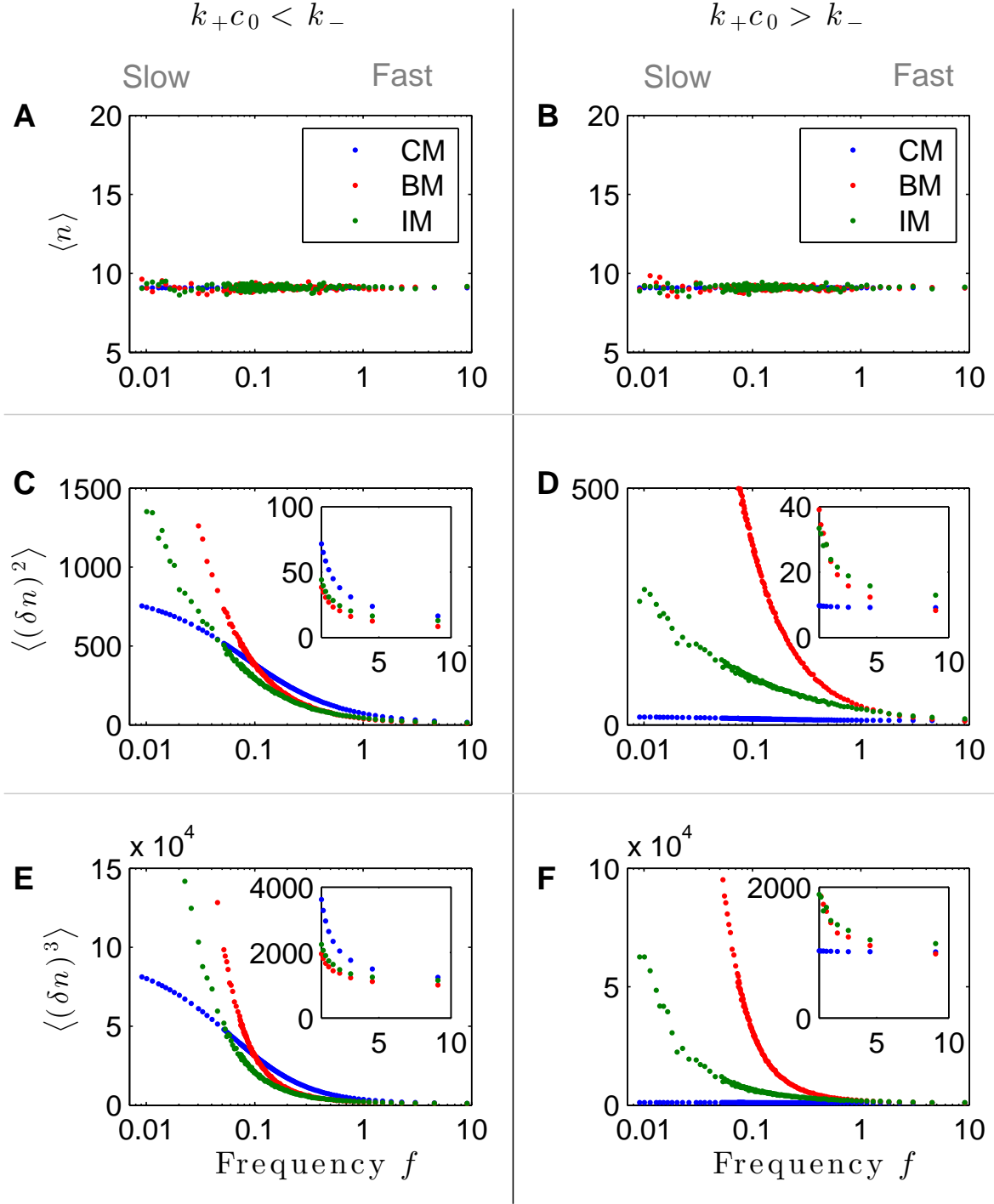
$$\frac{\langle \delta u(t) \delta u(t') \rangle_N^{FM}}{\left(\langle u(t) \rangle_N^{FM} \right)^2} = \frac{\langle \delta u(t) \delta u(t') \rangle_1^{BM}}{\left(\langle u(t) \rangle_1^{BM} \right)^2}. \quad (S79)$$

For slow dynamics, or fast dynamics with $k_{+c} > k_-$, CM is more accurate than BM. Hence, for N receptors, AM is even more accurate than FM. In contrast, for fast dynamics with $k_{+c} < k_-$, BM is up to twice as accurate as CM (Eq. (??)), and AM is N times more accurate than CM. Consequently, AM becomes more accurate for encoding than FM for more than two receptors (S6E Fig.). An exception are two receptors, for which AM and FM can be equally accurate (S6E Fig., inset). Since we generally show that larger signaling noise leads to larger output noise, the same rule emerges for decoding.

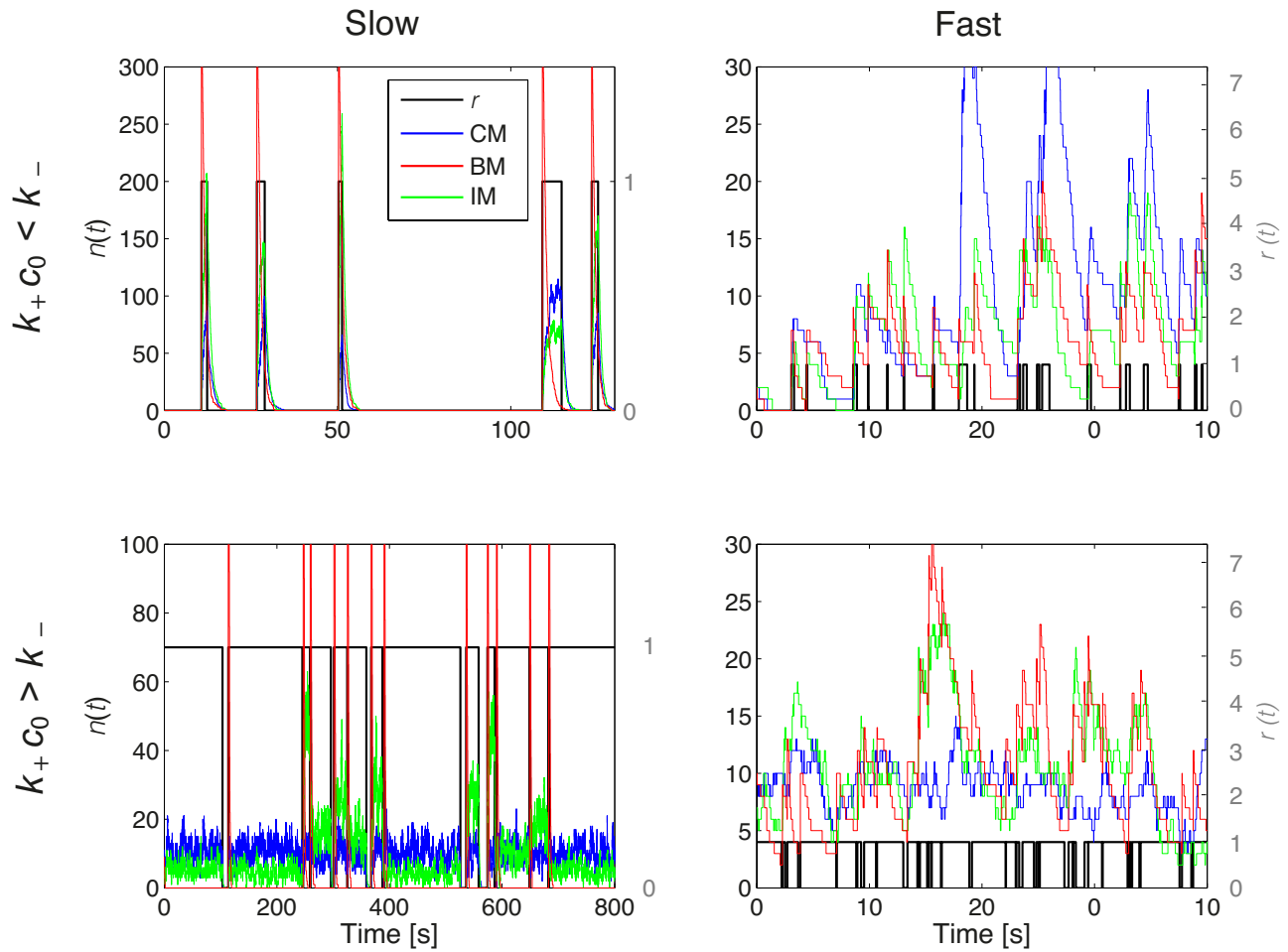
To extend our results to intermediate levels of synchronization for $N > 2$ receptors we consider a fraction ρ of synchronized receptors while the remaining fraction $(1 - \rho)$ are unsynchronized, with signaling either by CM or BM (S6E Fig.). When comparing CM and BM receptors for the same levels of synchronization ρ , BM receptors can remain more accurate than CM receptors (S6E Fig.). However, intermediate levels of synchronization do not strictly represent AM and FM. As shown in S6B,C Figs. synchronized CM receptors lead to pulses of variable duration, while unsynchronized BM receptors lead to highly frequent pulses with potentially variable amplitude.

Taken together, since single cells have thousands of receptors and ion channels, AM is the most accurate modulation scheme.

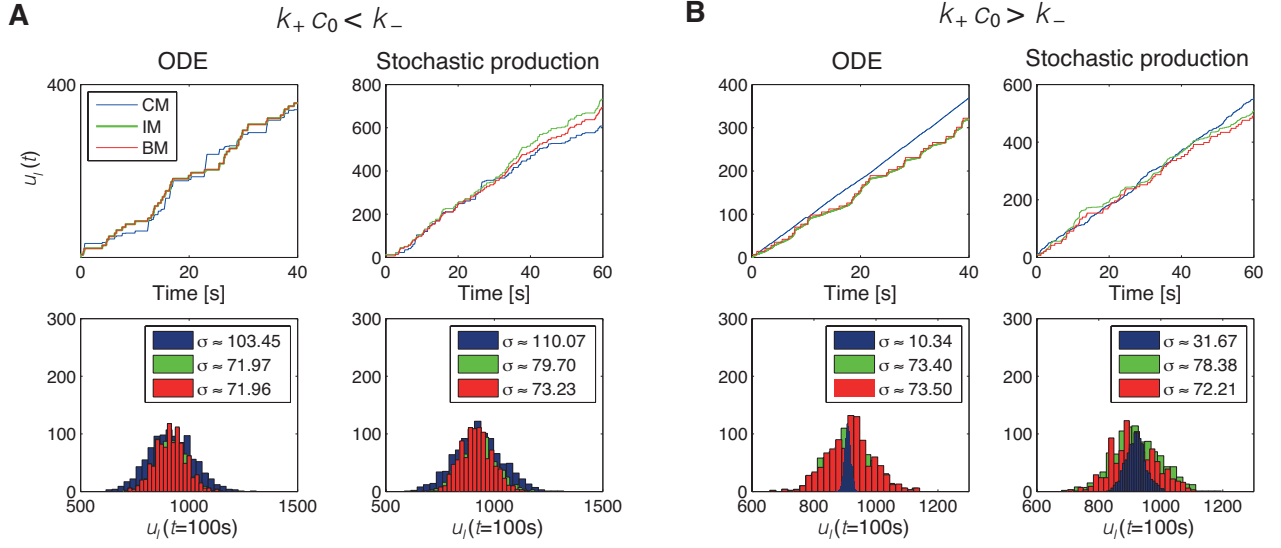
-
- [1] Mehta P, Schwab DJ (2012) Energetic costs of cellular computation. *Proc Natl Acad Sci U S A* 109: 17978-17982.
 - [2] Mora T, Wingreen NS (2010) Limits of sensing temporal concentration changes by single cells. *Phys Rev Lett* 104: 248101-248101.
 - [3] Endres RG, Wingreen NS (2009) Maximum likelihood and the single receptor. *Phys Rev Lett* 103: 158101-158101.
 - [4] Cai L, Dalal CK, Elowitz MB (2008) Frequency-modulated nuclear localization bursts coordinate gene regulation. *Nature* 455: 485-490.
 - [5] Hao N, O'Shea EK (2012) Signal-dependent dynamics of transcription factor translocation controls gene expression. *Nat Struct Mol Biol* 19: 31-39.



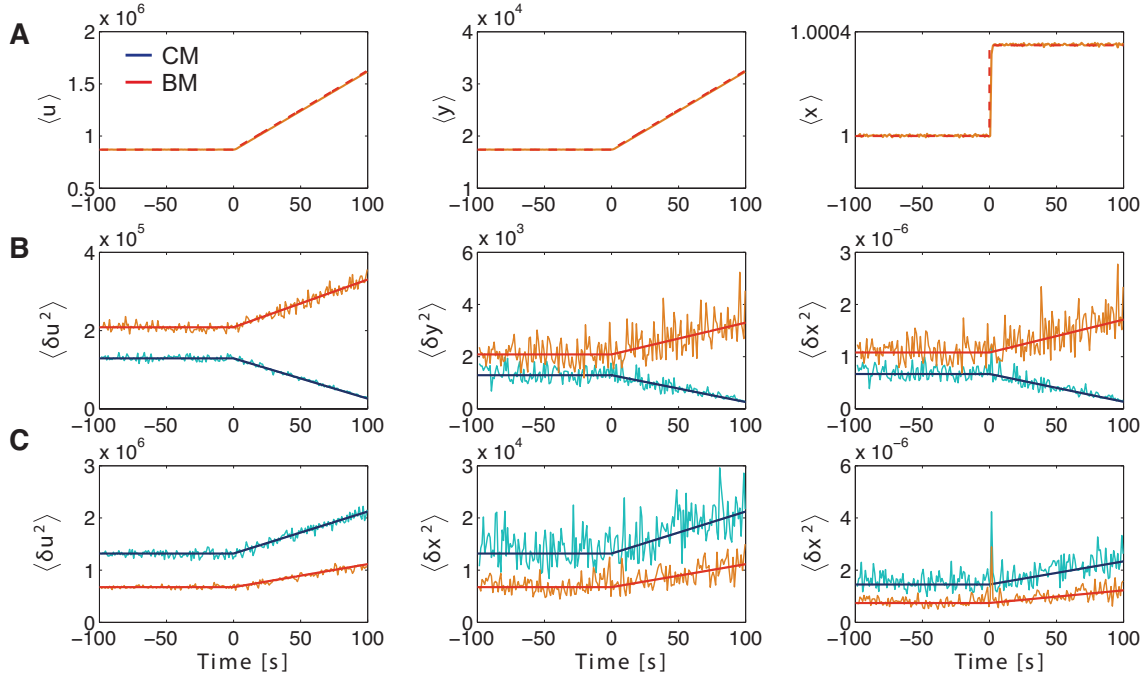
S1 Fig. **First three moments of the protein distribution in concentration sensing from the master equation.** Averages (A,B), variance (C,D), and skewness (E,F) as a function of the frequency of binding events, $f = k_{+c_0}/(1 + k_{+c_0}/k_{-})$. (Insets) Magnification of small-noise approximation region (fast switching). Analytical results for CM (blue) and numerical results for BM (red) and intermediate modulation IM (green) as function of the frequency of binding events (logarithmic scale). Note that this figure is similar to Fig. ?? in main text with the addition of IM. Two regimes are shown: $k_{-} = 10 k_{+c_0}$ ($\alpha = 100s^{-1}, \gamma = 1s^{-1}, \zeta$ from 1000 to 1) (left column) and $k_{-} = 0.1 k_{+c_0}$ ($\alpha = 10s^{-1}, \gamma = 1s^{-1}, \zeta$ from 1000 to 1) (right column). Averages from CM, BM and IM are constrained to be equal, *i.e.* ζ (BM) = αk_{-}^{-1} (CM) = $\alpha' \tau_b$ (IM). Variances of CM, BM and IM exhibit two different regimes for fast switching: for $k_{+c_0} < k_{-}$ BM is the most accurate mechanism and CM the worst (inset in C) while for $k_{+c_0} > k_{-}$ CM is generally the most accurate (except for $\zeta = 1$) and IM the worst (inset in D). Third moments show that, for large noise, the probability distributions become asymmetric.



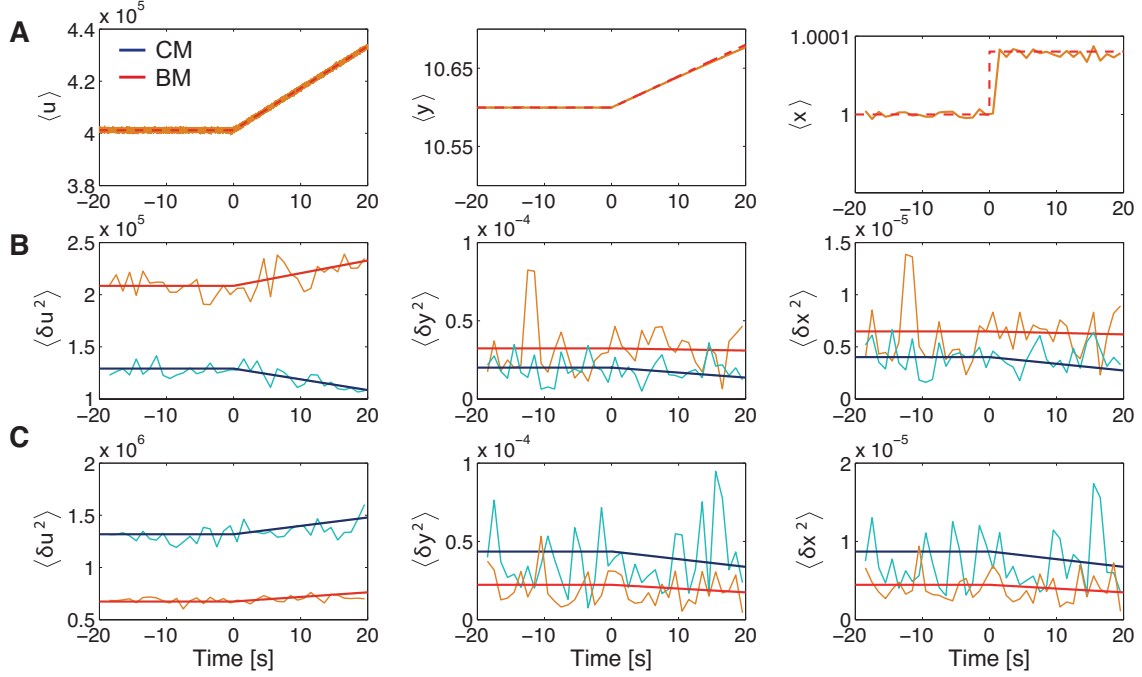
S2 Fig. **Examples of time traces of receptor activity and protein copy numbers for different regimes.** (Top) Regime $k_+c_0 < k_-$ with $k_+c = 0.1 k_-$ ($\alpha = 100s^{-1}, \gamma = 1s^{-1}$). (Bottom) Regime $k_+c_0 > k_-$ with $k_+c = 10 k_-$ ($\alpha = 10s^{-1}, \gamma = 1s^{-1}$). (Left) Slow switching with $\zeta = 400$. (Right) Fast switching with $\zeta = 7$. Receptor activity r and protein copy numbers $n(t)$ for CM, BM and IM are shown in black, blue, red and green, respectively.



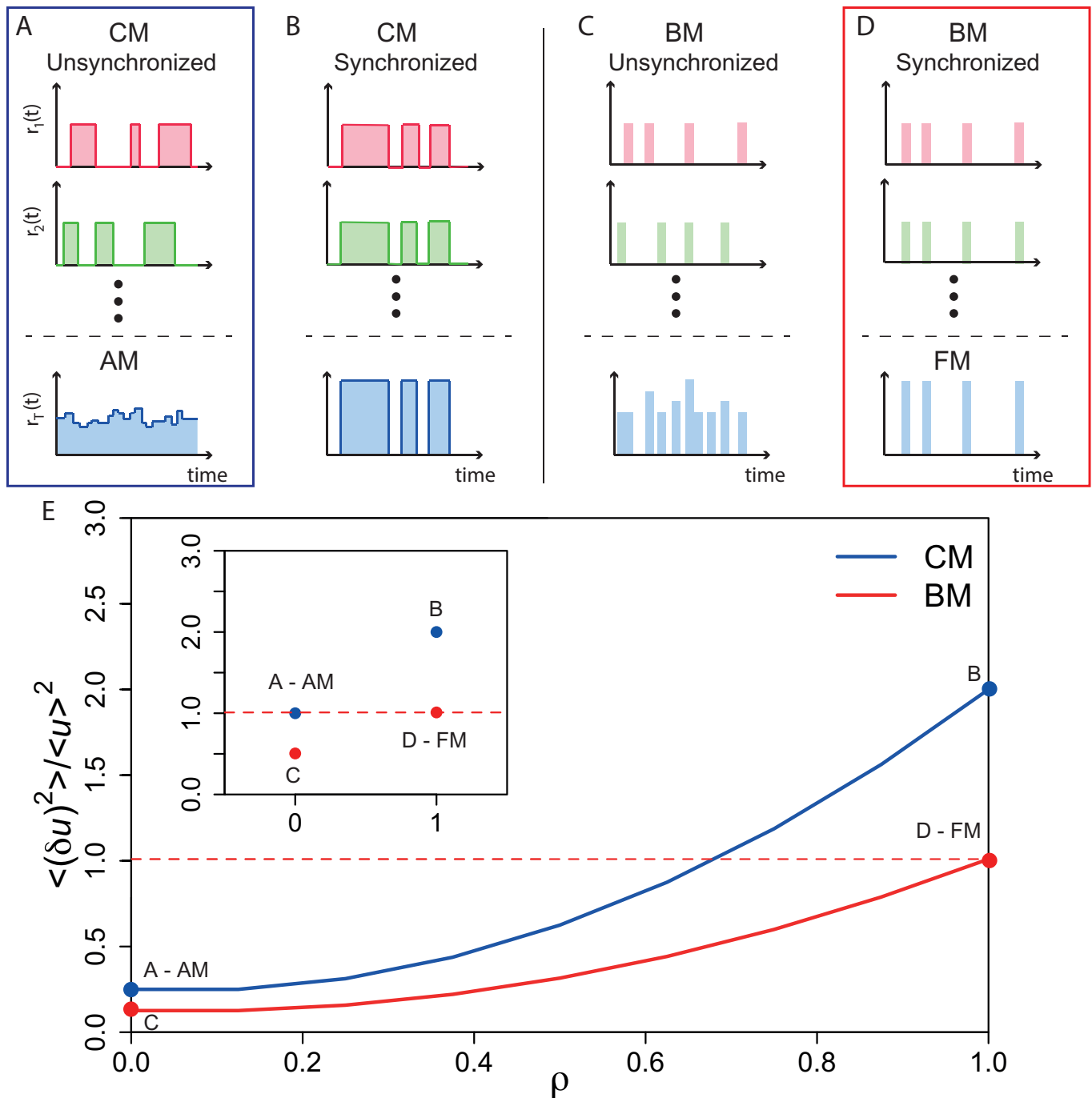
S3 Fig. **Investigating accuracy based on accumulative signaling (without protein production and degradation).** (A) Regime $k_+ c_0 < k_-$ with $k_+ c = 0.1 k_-$ ($\alpha = 100s^{-1}$, $\gamma = 1s^{-1}$ and $\zeta = 7$). (Left) ODE model. (Right) Stochastic protein production during τ_b in CM and IM. (Top) Examples of time traces. (Bottom) Histograms of number of proteins produced after 100s with standard deviation in legend based on 1000 simulations. (B) Analogous to (A) but for regime $k_+ c > k_-$ with $k_+ c = 10 k_-$ ($\alpha = 100s^{-1}$, $\gamma = 1s^{-1}$ and $\zeta = 7$). CM, BM and IM are shown in blue, red and green, respectively.



S4 Fig. **Incoherent feedforward loop: Comparison of analytical results with simulations of the stochastic differential equations.** (A) Averages of signaling rate u (left), species y from Eq. (S42) (middle) and species x from (S41) (right) as a function of time. Analytic solutions Eqs. (S32), (S43) and (12) are shown for BM in red, while a (time averaged) time-trace from a stochastic simulation using the Euler method is shown in orange (CM is almost identical and hence is not shown). (B) Corresponding variances as a function of time for $k_+ c_0 > k_-$ ($k_- = 6.7 \times 10^5 s^{-1}$, $k_+ c_0 = 10^6 s^{-1}$). Analytic results are shown in blue for CM and in red for BM; average over time (1s) from numerical simulations are shown in light blue for CM and in orange for BM. (C) Corresponding variances as a function of time for $k_+ c_0 < k_-$ ($k_- = 6.7 \times 10^6 s^{-1}$, $k_+ c_0 = 10^6 s^{-1}$). Colors same as in (B). Remaining parameters: $k_+ c_1 = 10^4 s^{-2}$, $k_x = 10s^{-1}$ and $k_y = 50s^{-1}$.



S5 Fig. **Integral feedback loop: Comparison of analytical results with simulations of the stochastic differential equations.** (A) Averages of signaling rate u (left), species y from Eq. (S60) (middle) and species x from (S59) (right) as a function of time. Analytic solutions Eqs. (S32), (S66) and (S65) are shown for BM in red, while a (time averaged) time-trace from a stochastic simulation using the Euler method is shown in orange (CM is almost identical and hence is not shown). (B) Corresponding variances as a function of time for $k_+c_0 > k_-$ ($k_- = 6.7 \times 10^5 s^{-1}$, $k_+c_0 = 10^6 s^{-1}$). Analytic results are shown in blue for CM and in red for BM; numerical simulations are shown in light blue for CM and in orange for BM. (C) Corresponding variances as a function of time for $k_+c_0 < k_-$ ($k_- = 6.7 \times 10^6 s^{-1}$, $k_+c_0 = 10^6 s^{-1}$). Colors same as in (B). Remaining parameters: $k_+c_1 = 10^4 s^{-2}$, $k_x = 10 s^{-1}$ and $k_y = 50 s^{-1}$.



S6 Fig. **From CM (BM) to AM (FM) for multiple receptors/ion channels.** (A-D) Schematic of receptor activity in time. (A) AM emerges from N unsynchronized receptors or ion channels in CM mode. (B) N synchronized CM receptors lead to a hybrid mechanism with information encoded in the frequency of broad bursts of variable duration. (C) N unsynchronized BM receptors provide a dense series of bursts. For large N , bursts may start overlapping, leading to variable amplitudes. (D) FM emerges from N synchronized receptors in BM mode. (E) Relative variance for a system of 8 receptors with ρN synchronized and $(1 - \rho)N$ unsynchronized receptors, plotted for fast dynamics in the $k_{+c} < k_{-}$ regime (CM in blue and BM in red). Letters refer to panel labels (A-D). Dotted red line indicates uncertainty from FM for comparison. (Inset) Same for a system of two receptors only.